Article, Online First

Herrling, Gerald; Becker, Marius; Lefebvre, Alice; Zorndt, Anna; Krämer, Knut; Winter, Christian

The effect of asymmetric dune roughness on tidal asymmetry in the Weser estuary

Earth Surface Processes and Landforms

Received: 2 March 2021 | Revised: 30 April 2021 | Accepted: 4 May 2021

DOI: 10.1002/esp.5170

RESEARCH ARTICLE

ESPL WILEY

The effect of asymmetric dune roughness on tidal asymmetry in the Weser estuary

Gerald Herrling[1] | Marius Becker[1] | Alice Lefebvre[2] | Anna Zorndt[3] | Knut Krämer[1] | Christian Winter[1]

[1]Institute of Geosciences Coastal Geology and Sedimentology, Kiel University, Kiel, Germany

[2]MARUM - Center for Marine Environmental Sciences, University of Bremen, Bremen, Germany

[3]BAW - Federal Waterways Engineering and Research Institute, Hamburg, Germany

Correspondence
Dr. Gerald Herrling, Institute of Geosciences | Coastal Geology and Sedimentology, Kiel University, Otto-Hahn-Platz 1, 24118 Kiel, Germany.
Email: gerald.herrling@ifg.uni-kiel.de

Funding information
Federal Waterways Engineering and Research Institute (BAW), Hamburg, Germany; Kiel Marine Science (KMS); German Research Foundation (DFG), Grant/Award Number: 345915838

Abstract

The bed of estuaries is often characterized by ripples and dunes of varying size. Whereas smaller bedforms adapt their morphological shape to the oscillating tidal currents, large compound dunes (here: asymmetric tidal dunes) remain stable for periods longer than a tidal cycle. Bedforms constitute a form roughness, that is, hydraulic flow resistance, which has a large-scale effect on tidal asymmetry and, hence, on hydrodynamics, sediment transport, and morphodynamics of estuaries and coastal seas. Flow separation behind the dune crest and recirculation on the steep downstream side result in turbulence and energy loss. Since the energy dissipation can be related to the dune lee slope angle, asymmetric dune shapes induce variable flow resistance during ebb and flood phases. Here, a noncalibrated numerical model has been applied to analyze the large-scale effect of symmetric and asymmetric dune shapes on estuarine tidal asymmetry evaluated by residual bed load sediment transport at the Weser estuary, Germany. Scenario simulations were performed with parameterized bed roughness of symmetric and asymmetric dune shapes and without dune roughness. The spatiotemporal interaction of distinct dune shapes with the main drivers of estuarine sediment and morphodynamics, that is, river discharge and tidal energy, is shown to be complex but substantial. The contrasting effects of flood- and ebb-oriented asymmetric dunes on residual bed load transport rates and directions are estimated to be of a similar importance as the controls of seasonal changes of discharge on these net sediment fluxes at the Lower Weser estuary. This corroborates the need to consider dune-induced directional bed roughness in numerical models of estuarine and tidal environments.

KEYWORDS
bedform roughness prediction, Delft3D, dune asymmetry, dune roughness, estuarine dynamics, estuarine tidal dunes, tidal asymmetry

1 | INTRODUCTION

Estuarine morphology is largely determined by residual sediment transport patterns that depend to a large extent on tidal asymmetry (Dronkers, 1986). Tidal asymmetry refers to the inequality between flood and ebb flow velocities and associated tidal phase durations, or the difference between slack water periods before ebb and flood (Dronkers, 1986). In estuaries, tidal asymmetry is governed by interacting mechanisms such as tidal wave dampening and distortion or tidal straining and estuarine circulation, to name a few, and has been extensively discussed in literature (e.g., Burchard et al., 2011; De Swart & Zimmerman, 2009; Dronkers, 1986; Friedrichs & Aubrey, 1988). The effect of directional hydraulic drag induced by large asymmetric tidal dunes has yet been given little attention in this discussion.

Bedforms, such as ripples, megaripples, or large dunes, cause a local hydraulic flow resistance, which has a large-scale effect on hydrodynamics and sediment dynamics of rivers, estuaries, and coastal seas (e.g., Blondeaux, 2012). Active tidal bedforms are defined as subaqueous flow transverse features, which significantly influence the flow field (Winter et al., 2015). The resistance to the flow induced by bedforms, that is, hydraulic bedform roughness, is associated with the flow expansion on their lee side resulting in kinetic energy loss, as exemplified for river dunes by Engelund and Fredsoe (1982). Additional turbulence generated in the case of flow separation behind the bedform crest and recirculation on the downstream side greatly enhances this effect (e.g., Vanoni & Hwang, 1967). The expansion loss and the rate of velocity decrease downstream of the bedform crest can be related to the lee slope angle (Best & Kostaschuk, 2002; Kwoll et al., 2016; Lefebvre & Winter, 2016; Motamedi et al., 2013; Paarlberg et al., 2007). While small bedforms such as ripples and megaripples are assumed to change their asymmetric orientation through morphological development with the oscillating tidal flow, large tidal dunes retain their morphological shape and orientation on time scales much longer than a tidal cycle. Consequently, lee slope angles of asymmetric dunes are different for reversing tidal flow and effective dune roughness changes between ebb and flood tidal phases. Field measurements of flow, turbulence, and transport patterns over large asymmetric dunes have revealed differences between tidal phases. For a tidal channel in the Danish Wadden Sea, Kwoll et al. (2014) showed that, when flow and primary bedform orientation are aligned (gentle stoss side facing the flow), water-depth-scale macroturbulent structures develop in the bedform lee-side, which are coupled to increased amounts of fine sediment in suspension. When flow and bedform orientation are opposed, no evidence of flow separation associated with primary bedforms was found. Lefebvre et al. (2011, 2013) found that asymmetric large primary bedforms are mainly contributing to form roughness, when the tidal flow is in alignment with dune asymmetry, that is, coming up the gentle stoss side and flow expansion and recirculation on the dune at the steep lee side. The effect of these findings on the estuarine scale, however, has not been shown yet.

Energy loss above bedforms must be considered in numerical hydro- and morphodynamic model simulations through bed friction coefficients that are associated with grain (i.e., skin friction) and bedform (i.e., form drag) roughness. In particular, the effect of form roughness on the flow has received little attention in large-scale model applications. Although computer power increases steadily, numerical coastal domain models are typically still restricted in horizontal and vertical grid resolutions to properly represent all topographical and morphological features; common grid cell sizes of process-based models are between 20 and 200 m. This implies the parameterization of the effect of bedform roughness elements that are of the dimension (dune lengths of 10–100 m) of a model grid cell or less. Thus, bedforms are usually considered as of "sub-grid-scale" (Sandbach et *al*., 2012). Even at high spatial resolution and adequate three-dimensional discretization of bedforms (and flow), their resistance to the flow is not necessarily accounted for. Flow separation and turbulence generation over bedforms require simulations with a fully nonhydrostatic model configuration (Lefebvre et al., 2014; Lefebvre & Winter, 2016). The use of nonhydrostatic models is computationally very intensive and still not applicable for large-scale coastal domains, which hence requires appropriate methods to parameterize the hydraulic effect of bedforms in, for example, numerical process-based models. Even more than for capturing flow properties, the correct parameterization of the effective bed roughness is crucial for the prediction of sediment transport. Although common in fluvial studies (e.g., Paarlberg et al., 2010), there are only few numerical model studies that apply bedform roughness predictors and deal with the effect of bedform drag on hydro- and morphodynamics at the estuarine and coastal system scales (e.g., Brakenhoff et al., 2020b; Davies & Robins, 2017; Herrling et al., 2017; Villaret et al., 2011, 2013; Wang et al., 2016).

The form resistance exerted by bedforms, caused by local flow separation and recirculation, depends on bedform dimension, flow, and sediment characteristics (Karim, 1999). Hydraulic bedform roughness predictors are usually based on the ratio of height and length (i.e., steepness) of a bedform (Julien & Klaassen, 1995; Karim, 1999; van Rijn, 1984; Yalin, 1964) and thus require field data or a prediction of bedform geometry. Yet the predictor of van Rijn (2007a) directly expresses the bedform roughness height depending on flow velocity, sediment grain size, and water depth. Thus, in tidal environments, variations of current speed and water depth may result in variations of bedform roughness over a tidal cycle. However, since primarily developed for unidirectional flow, van Rijn (2007a) disregarded the asymmetrical geometry of tidal dunes that results in exposures of different lee slope angles during reversing tidal flows. A modified application of van Rijn's (2007a) dune roughness predictor here considers the directionality of bedform roughness induced by asymmetric tidal dunes.

The objectives of the present study are twofold. The first is to determine the effect of asymmetric dune shapes parameterized through tidal-phase-dependent bed roughness on spatiotemporal flow and sediment transport at the Weser estuary. The second is to discuss the combined effects of freshwater discharge, tidal energy conditions, and dune-induced flow resistance on the estuarine tidal asymmetry. Several different harmonic and statistical methods exist to characterize tidal asymmetry (Guo et al., 2019). Here, the tidal asymmetry is shown by the direction and magnitude of residual bed load sediment transport, because of the specific role of bed load controlling both local bedform-related (Naqshband et al., 2014) and large-scale changes of estuarine morphology.

2 | STUDY AREA

2.1 | Weser estuary

The Weser estuary is located at the southeastern coast of the North Sea, Germany, (Figure 1a) and can be classified as partially mixed (Grabemann & Krause, 1989). The distance from the tidal barrier at Bremen-Hemelingen (km −5) to the mouth of the estuary (km 112) where the main channel opens into North Sea waters is 117 km (Figure 1b). The official kilometrage of the navigation channel starts at Bremen Weserbrücke (km 0). In the following, the distance to the upstream tidal barrier at Hemelingen is marked by −5 km. The estuarine reach can be subdivided into the Lower Weser (Hemelingen to Bremerhaven, km − 5 to 67) and the Outer Weser downstream from Bremerhaven to the open North Sea. At the Outer Weser, several channel–shoal systems with large intertidal areas drain into the

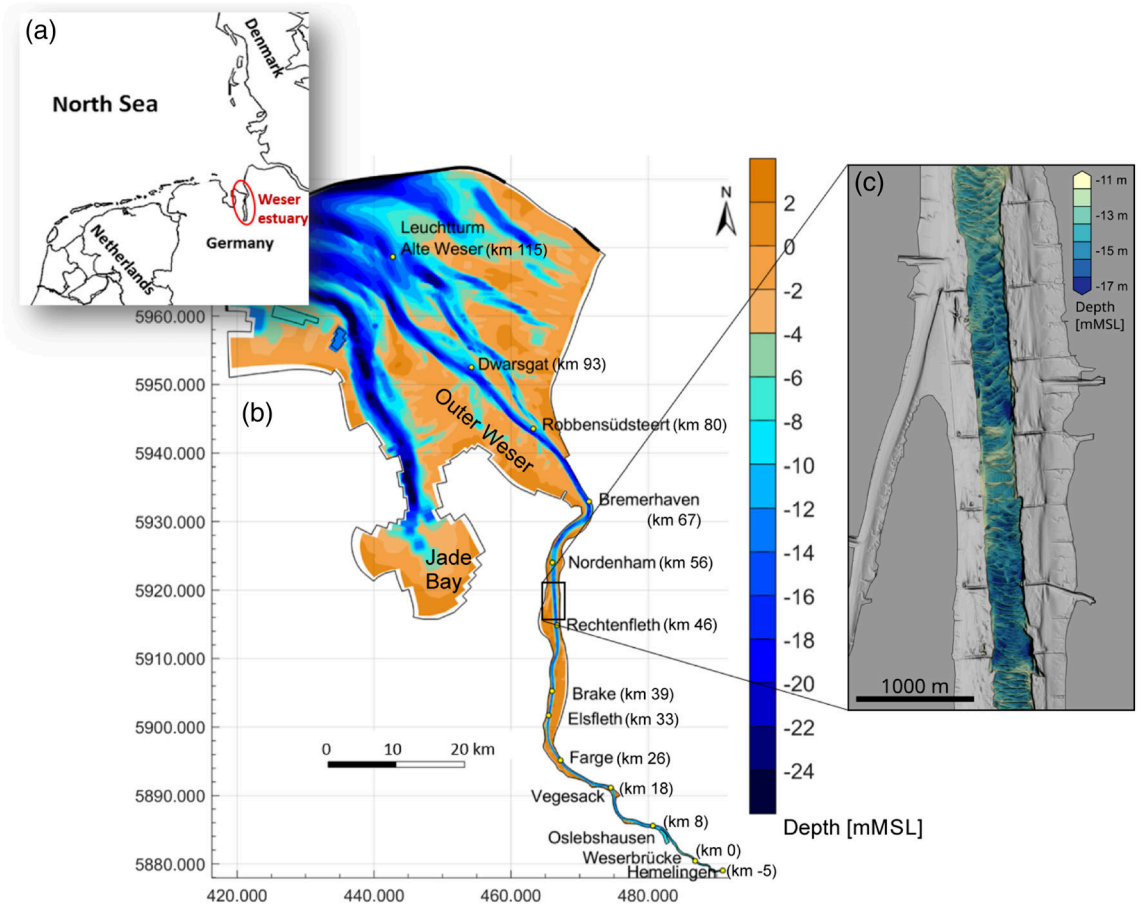

FIGURE 1 The Weser estuary in the southeastern North Sea, Germany (a). The model from the tidal barrier at Bremen-Hemelingen to the mouth of the estuary (b). Visualization of typical tidal dunes (c) measured by high-resolution (2 × 2 m) bathymetrical surveys of the waterways and shipping authorities of Bremen and Bremerhaven. Water level gauges are depicted by dots with names and Weser km

estuarine channel. The estuary is characterized as mesotidal with tidal range increasing upstream from 2.9 m at the mouth (km 112) to 4.2 m at Bremen (km 0). The mean water depth along the navigational channel increases from approximately 6 m at Bremen to up to 22 m at the Outer Weser (Figure 2b). The channelized fairway, with an almost constant width of 200 m between Bremen (km 0) and the port of Brake (km 39), there abruptly expands to a width of approximately 300 m.

The sedimentology of the channel bed is characterized by medium to coarse grained sands with locally high amounts of cohesive sediments (Figure 2a). Grain sizes are variable along the navigational channel with lowest values to be found in the estuarine turbidity maximum zone (ETM) from km 56 to 73. The cohesive sediment content in the main channel is largely below 25%, except for local peaks of 50–75% along the port of Bremen (km 5–8) and at the estuarine turbidity maximum. Intertidal flats flanking the channel at the mouth of the estuary are mainly composed of fine to very fine grained sands. Statistics of freshwater discharge for the years 1941–2017, that is, mean of the observed low discharges (MLQ), annual mean (MQ), and mean of the observed high discharges (MHQ), measured at Intschede at the riverine part upstream of the tidal barrier are 123, 319, and 1,220 m^3/s, respectively.

2.2 | Evaluation of tidal dune characteristics

Regular monitoring of the navigational channel and maintenance dredging are carried out by the local authorities (Waterways and Shipping Authorities of Bremen and Bremerhaven). High-resolution (2 × 2 m) multibeam bathymetric data (see example Figure 1c) was processed by filtering and zero-upcrossing methods (Krämer et al., 2019). Dune parameters are calculated for spatial dune data segmented in along channel beds with lengths of 500 m and cross-channel widths of approximately 200 m depending on spatial coverage of the measurements. Dune dimensions, asymmetry, and lee-side angles were determined for two characteristic morphological states in April 2009 after a moderate discharge event of up to 750 m^3/s and in September 2009 after months of low discharge with less than 200 m^3/s (Figure 2c–g).

The dune length is here defined as the distance between two consecutive troughs. The dune height was calculated as the distance of the crest from a straight line connecting two troughs, determined as a vertical line through the crest. Bedform asymmetry is determined as the length of the ebb stoss side (facing the ebb stream) to the total length of the dune (A_d > 0.5 ebb-directed asymmetry and A_d < 0.5 flood-directed asymmetry). The hydraulically relevant steep segment of the dune lee slope, that is, the slip face (Lefebvre et al., 2020; Lefebvre et al., 2016), is here determined as the maximum dune lee-side angle for flow directions during ebb and flood, respectively. Slip-face angles of 11° are considered an onset for initiation of flow separation, while fully developed and persistent flow separation and maximum hydraulic flow resistance is expected for lee-side angles steeper than 24° (Kwoll et al., 2016; Lefebvre & Winter, 2016). In view of the diversity of natural dune shapes, characteristic values for

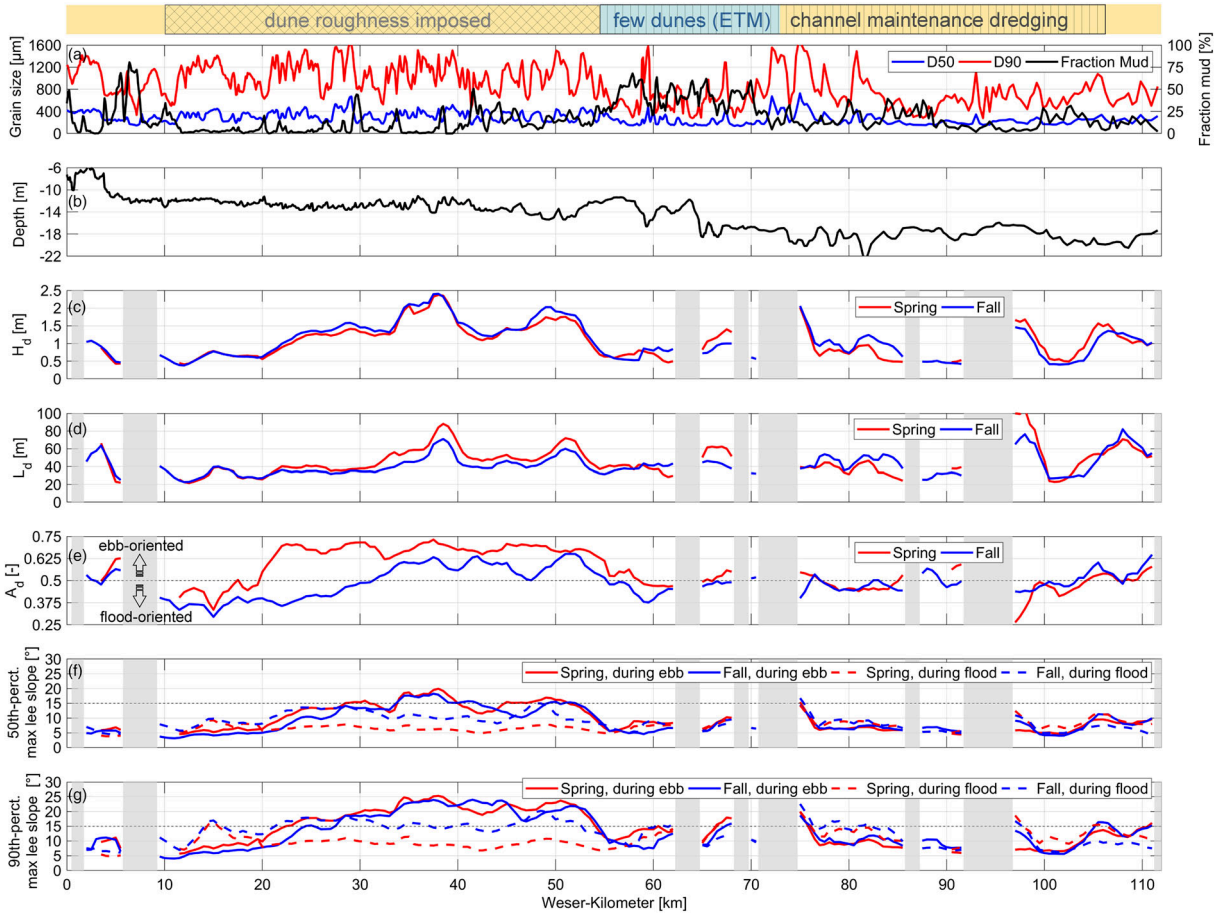

FIGURE 2 Observed surface sediment grain-size characteristics (a) and channel water depth (b) along the navigational channel from Bremen (km 0) to the mouth of the estuary (km 112). Measured dune dimension and geometry: Median dune height H_d (c), median dune length L_d (d), median dune asymmetry A_d (e), 50th-percentile maximum dune lee slope (f) and 90th-percentile maximum dune lee slope (g) in spring 2009 after high discharge and fall 2009 after months of low-discharge regime. Data were not available for sections depicted in gray

these maximum angles are determined as follows. First, the maximum angle is obtained from along channel bed elevation profiles, as it occurs locally along the lee side of each dune. Then, for all dunes found in along-channel segments of 500 m, the 50th (median) and the 90th percentile of these local maximum angles are calculated, that is, per segment 50% (or 90%, respectively) of all dunes obtain a smaller local maximum angle.

Dune dimensions vary along the navigational channel with median dune heights ranging between 0.5 and 2.5 m and median dune lengths between 20 and 100 m (Figure 2c,d). Dune crest orientation was found to be perpendicular to the main flow direction at the channelized cross-section (Lefebvre et al., 2020). In the Lower Weser from km 20 to 55, large tidal dunes are identified to be mostly ebb-oriented (asymmetry > 0.5) with gentle stoss sides facing towards the ebb current and steep lee sides particularly after high discharge events as, for example, seen for spring 2009 (Figure 2e). Although many dunes at this reach are ebb-oriented, also symmetrical (asymmetry ~0.5) and even flood-oriented (asymmetry < 0.5) dunes are observed between km 10 and 33 in fall after times of low discharge ranging between 100 and 200 m^3/s in summer. Downstream of km 55, tidal dunes are found to be symmetrical to partially flood-oriented irrespective of the discharge regime. Their maximum lee-side angles are gentle and exceed median values of 11° or 90th percentile ranks of 15° only sporadically, and thus, dune-induced form roughness is assumed to be hydraulically not relevant in this study (Figure 2f,g). At the upper estuary between km 20 and 55, however, these thresholds are exceeded, in particular during ebb tidal phases. Maximum lee-side angles mostly between 11° and 15° suppose flow separation to be initiated for 50% of the dunes (50th percentile). For 10% of the dunes (90th percentile), maximum lee-side angles exceed 15° and are locally up to 25°. Here, flow separation, turbulence, and, thus, form drag are supposed to be more frequent and well developed. Furthermore, these tidal dunes are found to change their morphological shape and asymmetry with seasonal variations of discharge regime (km 10–55).

The variability and extent of these bedforms motivated us to this idealized study that aims to evaluate the effect of different dune shapes and roughness parameterizations on tidal asymmetry.

Findings, here derived from data limited to two morphological states in spring and fall 2009, are supported by the analysis and interpretation of extensive spatiotemporal data of tidal dunes in the Weser estuary (Lefebvre et al., 2020).

3 | METHODOLOGY

3.1 | Model setup

The modeling system Delft3D (Deltares, 2014) has been applied to set up and run process-based models in a baroclinic, three-dimensional (3D) configuration to simulate hydrodynamics and

sediment transport in the Weser estuary. The modeling system solves the horizontal momentum equations, the continuity equation, and the transport equation on a staggered model grid by use of an implicit finite-difference scheme. The evolution of turbulent flow is simulated by the application of the k-ϵ turbulence closure model. For a detailed description of the equations and implementation into Delft3D, the reader is referred to Lesser et al. (2004) or the documentation distributed with the modeling system (Deltares, 2014).

The Weser model covers the estuary from the tidal barrier at Bremen-Hemelingen and extends seawards to coastal water depths of 25 m (Figure 1b). Here, water level boundary conditions were prescribed by nesting into the larger process-based EasyGSH-model covering the North Sea (Hagen et al., 2019). The Weser model is structured by a curvilinear grid that was set up with an increased resolution in the main estuarine channel. The cross-channel resolution is 60 m at the mouth, increasing to 10 m at the upstream end of the estuary by narrowing of curvilinear grid lines. Along-channel resolution likewise increases in upstream direction from 400 to 50 m with locally twofold higher resolution in river bends. Less focus was set on the Outer Weser and Jade Bay intertidal flats where the size of the grid cells is in the order of 500 m and locally up to 1,500 m at the domain margins. Eleven terrain-following sigma layers resolve the vertical dimension of the model grid. The vertical discretization is not equidistant and approaches a logarithmic profile with layer thicknesses relative to the local water depth of only 2% at the bottom and up to 15% close to the water surface.

Bathymetric surveys were conducted by the local authorities using multibeam echo sounders for subtidal areas and airborne laser scanning for intertidal flats and marshes between the years 2010 and 2012 (Waterways and Shipping Authorities at Bremen and Bremerhaven). A digital elevation model (DEM) covering the entire estuary was generated from interpolating measured bathymetric data onto a rectangular grid with raster sizes of 5 m (https://www.kuestendaten.de/Tideweser/DE/Service/Kartenthemen/Kartenthemen_node.html). Data from this high-resolution DGM were interpolated onto the model grid by using depth averaging within each model grid cell (Figure 1b and Figure 2b).

Samples of sediment grainsize composition (Milbradt et al., 2015; Valerius et al., 2015) available in 12 sediment grain-size classes from cohesive sediments to very coarse sand of 2,000 μm were used to determine an initial sediment distribution of the Weser model. Samples were collected at channel cross-sections that each were distanced by 250 m downstream. The sampling density was lower on intertidal flats at the estuarine mouth. The original sediment distributions of 12 sediment classes were clustered to five sand classes and one cohesive sediment class. Considering the area of the Lower Weser estuarine channel (km 0–70), mass-weighted mean grain sizes were determined for individual sand classes, that is, 91, 182, 302, 501, and 1,232 μm. The sand fraction with a mean grain size determined to be 501 μm, for example, was merged from two original sand classes: (1) 354–500 μm with mean grain size of 427 μm and relative total mass of 9.75% and (2) 501–707 μm with mean grain size of 604 μm and relative total mass of 7.06% (calculated as: $0.0975/(0.0975 + 0.0706) \times 427\ \mu m + 0.0706/(0.0975 + 0.0706) \times 604\ \mu m = 501.3\ \mu m$). Its mass is thereby determined as the total mass of the original classes merged into this new fraction. The distribution of each sediment fraction is accounted for as mass percentages at bed cells in the model.

Van Rijn's (2007b) transport formula, as implemented in the modeling system, is applicable only for sand fractions ≥100 μm. For this reason, the smallest determined sand fraction with a mean grain size of 91 μm is prescribed in the model as 100 μm. Percentiles from grain size distribution, that is, D50 and D90 (Figure 2a), were calculated from composition and spatial distribution of five sand fractions incorporated to the model. The availability of a specific grain size fraction, that is, mass percentage at a grid cell, is accounted for by a factor that controls the sediment transport rate. Although the transport formula applied (Van Rijn, 2007b) computes suspended and bed load sediment transport, only the sediment part that is transported by bed load processes is considered for the subsequent analysis. Our study is on time-averaged residual bed load sediment fluxes that were shown to especially contribute to dune morphodynamics and migration (Naqshband et al., 2014). The feedback between high suspended sediment concentrations and the effective hydraulic drag in estuaries (Winterwerp, Lely, & He, 2009) and the effect of dune morphology on dynamics of very fine sediments (e.g., Kwoll et al., 2013) or vice versa, that is, the contribution of suspended sand to dune morphology (Hendershot et al., 2016; Kostaschuk & Best, 2005), are neglected in this study.

For the definition of hotstart conditions, preceding simulations were performed allowing for a sufficiently long spin-up to establish realistic horizontal salinity gradients along the estuarine reach and to smooth the initially prescribed sediment distribution. These salinity gradients and spatial sediment distributions were used to initiate subsequent simulations to be evaluated.

A plausibility test was conducted to verify whether the uncalibrated model meets expectations. Water levels and salinity concentrations were simulated from April 2 to May 2, 2009, and compared with observations at 13 water level gauges and at 10 salinity gauges maintained by the local authorities (see Figure 1 for the position of water level gauges). Salinity concentrations are surveyed at water depths of approximately 1 m below mean low water level. Root mean square errors (RMSEs) between measured and modeled water levels are 0.1 m at the mouth of the estuary (km 115), <0.25 m at the outer, and <0.15 m at the inner estuary. Simulated salinity concentrations are compared with observations by RMSEs <2.2 psu at the outer estuary, <0.5 psu at the spatial range of the estuarine turbidity maximum, and <0.1 psu upstream from there. For this plausibility test, measured freshwater discharge was imposed, and bed roughness coefficients parameterizing the frictional drag of symmetric dunes (Sections 3.3 and 3.4) were prescribed. The spatiotemporal variability of water levels and salinity gradients was assumed to be sufficiently represented by the model. Model quality was thus accepted to be good enough for the subsequent parameter study.

3.2 | Scenario simulations

This schematic study investigates the effect of bedform asymmetry on flow characteristics and estuarine tidal asymmetry. Twelve scenario simulations were run to distinguish between the effects of four different dune roughness parameterizations (Sections 3.3 and 3.4) and of constant upstream discharges of 150, 450, or 750 m^3/s on hydrodynamics and sediment transport (Table 1). Characteristic discharges of a flood event in March/April 2009 (750 m^3/s) and typical summer

TABLE 1 Twelve scenario simulations were conducted with four different dune roughness parameterizations (Sections 3.3 to 3.4) and three different discharges. This overview indicates where outputs of these 12 simulations are presented

	No dunes, that is, dune roughness deactivated	Ebb-oriented asymmetrical dunes, that is, dune roughness activated for ebb phases	Symmetrical dunes, that is, dune roughness activated for ebb and flood phases	Flood-oriented asymmetrical dunes, that is, dune roughness activated for flood phases
Discharge of 150 m^3/s	**1**: Figure 6a (black)	**2**: Figure 6a (blue)	**3**: Figure 6a (red)	**4**: Figure 6a (green)
Discharge of 450 m^3/s	**5**: Figures 4a, 5abc, 6b, 7, A1–A4 (black)	**6**: Figures 4b, 5abc, 6b, 7, A1–A4 (blue)	**7**: Figures 4c, 5abc, 6b, 7, A1–A4 (red)	**8**: Figures 4d, 5abc, 6b, 7, A1–A4 (green)
Discharge of 750 m^3/s	**9**: Figure 6c (black)	**10**: Figure 6c (blue)	**11**: Figure 6c (red)	**12**: Figure 6c (green)

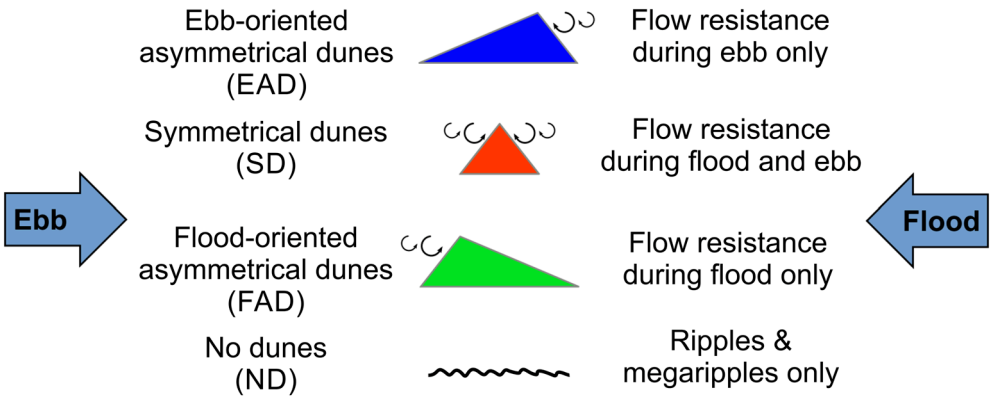

FIGURE 3 Illustration of different dune roughness scenarios parameterized in the model by predicted bed roughness coefficients. The color code of depicted bedforms is adopted in Figures 5–7

and autumn rates of 150 m^3/s are complemented by a third discharge regime of 450 m^3/s to reveal the transition between low to high discharge conditions. The simulations cover a neap-to-spring period of 15 tidal cycles between April 4 and April 11, 2009. The first tidal cycle served as an additional spin-up and was disregarded for the subsequent analysis.

The focus here is on along-channel residual bed load sediment transport (RBLT). Fluxes of RBLT ($m^3/s/m$) integrate the mass of all sand fractions (specific and dry bed density of 2,650 and 1,600 kg/m^3) being transported during 14 tidal cycles and were determined along grid cells between five curvilinear grid lines following the largely channelized bed of the fairway. These slightly diverging grid lines were purposely aligned to cover the deeper cross-sectional part of the channel bed that itself keeps widening in downstream direction. Note that the residual sediment transport ($m^3/s/m$) integrates the flux of the sediment mass per unit width, irrespective of the cross-sectional area that was taken into account for spatiotemporal integration. Sediment fluxes perpendicular to the channel orientation, for example, due to secondary currents in river bends, were not taken into consideration when computing along-channel RBLT.

3.3 | Different dune shape and roughness parameterizations

Tidal dunes in the Weser estuary, with typical heights ranging between 1 and 2 m and lengths between 40 and 70 m, are those primary bedforms that retain their asymmetric shape and orientation throughout tidal cycles and even on time scales of weeks and months (e.g., Lefebvre et al., 2020). For reversing tidal flow, form drag is thus assumed to be only effective when the flow is in line with the dune asymmetry, that is, converging on the gentle stoss side and diverging on the dune at the steep lee side.

Consequently, roughness parameterized for asymmetrical dunes varies between ebb and flood tidal phases; for example, ebb-oriented dunes (EAD) are considered hydraulically active during ebb only. The opposite goes for flood-oriented asymmetrical dunes (FAD), where dune roughness is active during flood only. Symmetrical dune shapes (SD), here assumed to induce form drag through flow separation and turbulence at both flanks of the dune, are parameterized by effective dune roughness during the full tidal cycle. Dune-induced roughness is deactivated for a fourth scenario: "no dunes" (ND). According to that, the effects of four different dune roughness parameterizations are distinguished (Figure 3).

Ripple and megaripples, which are often superimposed to large tidal dunes, are assumed here to be hydraulically active independent of the tidal flow direction (Section 3.6).

In nature, different dune shapes are observed in the main channel, predominantly symmetric dunes in the outer part and ebb-oriented, symmetric, or flood-oriented in the inner part of the estuary (Figure 2e). For the sake of simplicity and to better distinguish the effects of individual dune shapes on tidal asymmetry and bed load sediment fluxes along the estuary, we refrain from schematizing mixed dune shapes for one and the same scenario simulation. Each simulation represents one distinct dune shape, that is, dune roughness parameterization.

3.4 | Inter-tidal-phase variable dune roughness

Dune roughness height prediction (Section 3.5) is either activated or deactivated for individual tidal phases depending on the schematized dune shape (Figure 3). During slack tide when the tide turns, current speed is very low and there is no relevance to dune roughness. This circumstance justifies the method of connecting individual model runs of flood and ebb phases applying continuous boundary conditions from April 4 to 11, 2009. Thereby, each model run is conducted for one tidal phase, that is, from one slack tide to the next one, while being continued from the final time step output of a previous run at slack tide. At each slack tide, the dune roughness is changed to match the tidal phase that is executed. The ineffective dune roughness at slack tide ensures a smooth alteration without the risk of abrupt changes to the flow. A batch file executes this sequence of model runs of successive tidal phases. This approach allows a timely variation of the bedform roughness between tidal phases, which is not yet incorporated in the modeling system Delft3D. Outputs of all batched runs of individual tidal phases were recomposed before relevant metrics were calculated from the model output of the scenario simulations.

The effective times of slack tide used to separate individual model runs were appointed from processing the output of a continuous simulation of 14 tidal cycles with the parameterization of symmetric dunes, that is, dune roughness activated during the full tidal cycle. Instants of slack tide were determined from minima of near-bed flow velocity computed at mid-channel grid cells. These instants of slack tide were spatially averaged along a preselected dune field from km 10 to 55. Note that tidal-phase-dependent dune roughness is only imposed at this dune field (Section 3.5). This appoints 29 (spatially averaged) instants of slack tide for 14 tidal cycles.

The time period of the tidal wave propagating along this dune field of 45 km varies between 10 and 90 min depending on the respective tidal phase and discharge regime. Accordingly, the maximum phase lag between local instants of slack tide at the upstream and downstream extremities of this reach and the spatially averaged instant of slack tide is approximately half that period, that is, 5–45 min. Thus, shortly after slack tide and solely for asymmetrical dune parameterizations, there could be a mistimed prescription of dune roughness. Time series of water level, combined bed roughness, velocity, and bed load sediment transport are shown for Weser km 33 and 54 at the center and at the downstream end of the dune field from km 10 to 55 (Figures A1 and A2, see appendix). A smooth transition between ebb and flood tidal phases of these parameters is accomplished at both locations for scenario simulations with asymmetric dune roughness, which confirms the robustness of this method.

3.5 | Dune roughness height prediction

Dune morphology, and how it varies in time and space, has strong effects on bedform roughness height. After Warmink et al. (2013), bedform roughness predictors can generally be classified into analytical, semianalytical, and empirical roughness approaches: analytical predictors (e.g., Yalin, 1964) are directly based on the mass and momentum conservation laws; semianalytical roughness predictors (e.g., Karim, 1999) on the conservation laws, but are calibrated to fit data from flume experiments; and empirical roughness predictors (van Rijn, 1984, 2007a; Vanoni & Hwang, 1967) rely on empirical relations between bedform and flow characteristics and measured bed roughness.

van Rijn (2007a) bedform roughness predictor as applied here directly determines the ripple-, megaripple- and dune-induced roughness coefficients governed by dynamically simulated water depth, flow velocity, and median grain size. Van Rijn's bedform roughness predictor (2007) and particularly the dune roughness predictor have primarily been developed for steady, riverine conditions. The scheme has already been applied in large-scale coastal area models and appears to be robust (Davies & Robins, 2017; Herrling et al., 2017; Villaret et al., 2011, 2013; Wang et al., 2016). A recent study (Herrling et al., 2019) explored the parameterization of bedform hydraulic roughness in a model (Delft3D) of the Weser estuary. Well-established bedform roughness predictors of van Rijn (2007a, 1984) were related to observations of dune dimension evaluated from high-resolution bathymetrical surveys of a dune field at the upper Weser estuary. The dune roughness prediction after van Rijn (2007a) gave a satisfactory representation of the bed friction, while its predecessor (van Rijn, 1984) underestimated dune-induced roughness. Both predictors had been evaluated following van Rijn's expectation that the dune roughness height (Nikuradse, k_s) should be "on the order of half the dune height."

In the present study, van Rijn's (2007a) dynamic bedform roughness height prediction is only used in a predefined channelized area (km 10–55) in which hydraulically relevant dunes are existent. The selection of this dune field is determined based on a combination of observed dune characteristics: (i) dune dimension, (ii) steepness of the maximum lee-side angle, and (iii) the connectivity of the dune field. From km 60 to 107, approximately, channel maintenance dredging and cutting of dune crests occurs regularly so that large tidal dunes with steep lee-side faces are only found sporadically, such as at km 75 (Figure 2g). Aside from that, the development of large bedforms is prevented by high amounts (~50%) of cohesive sediments at the channel bed within the spatial range of the estuarine turbidity maximum (km 56–73, Figure 2a, see also Becker et al., 2013). Therefore, dune roughness prediction is spatially restricted to the dominant dune field in the estuarine channel between km 10 and 55 (Figure 2c–g).

It should be noted that channel widths are up to 1 km at the Outer Weser. Residual flow and sediment transport can be variable across this width, which is attributed to secondary currents at channel curvatures or estuarine processes affecting the lateral distribution of flow intensity and, hence, the emergence of bedforms. Potential dune fields of small extent that are scattered at the outer channel margins were not covered by the data collected along mid-channel but are supposed to contribute only small effective friction. These processes are of subordinate importance along the constricted channel bed and dune field in the Lower Weser where parameterized dune roughness was prescribed.

To account for the effect of different dune roughness parameterizations between km 10 and 55, the dynamic dune roughness prediction is either activated or deactivated for particular tidal phases (Sections 3.3, 3.4 and Figure 4). The computation of depth-averaged flow velocity and instantaneous bed load sediment transport is shown to be dependent on this inter-tidal-phase variable dune roughness (Figures A3 and A4, see appendix).

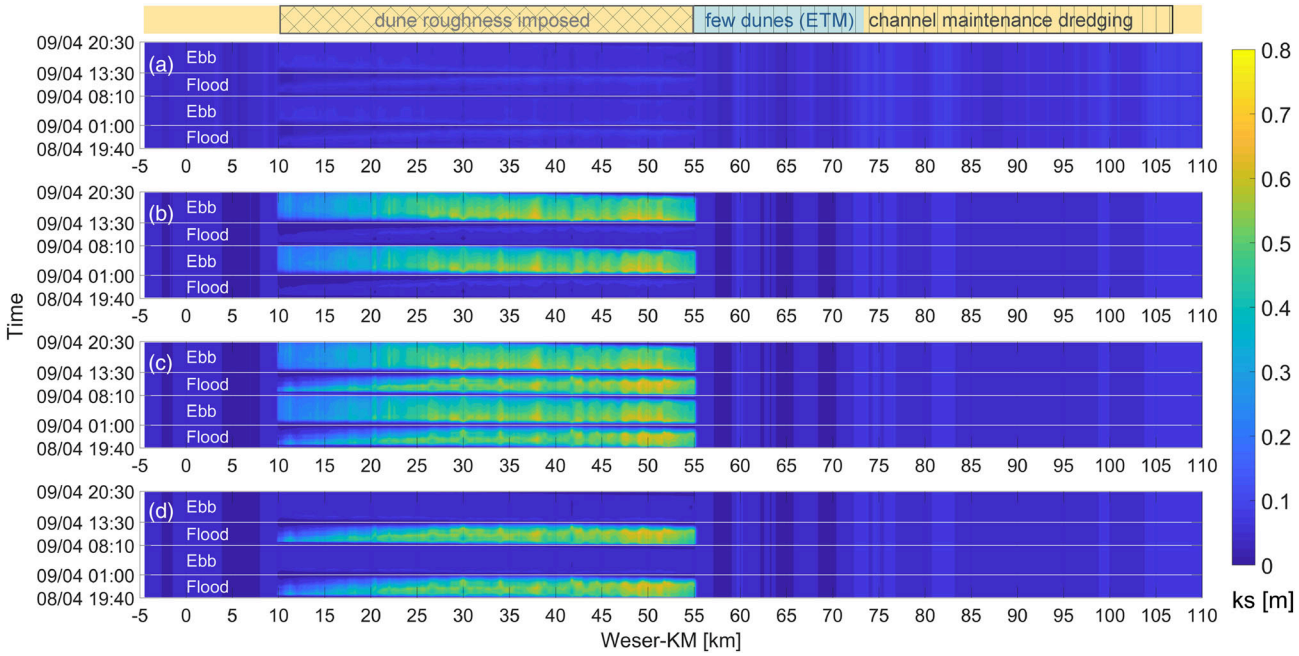

FIGURE 4 Combined bed roughness (Nikuradse, k_s) applied for scenario simulations considering "no dunes" (a), "ebb-oriented asymmetrical" (b), "symmetrical" (c), or "flood-oriented asymmetrical dunes" (d) along the estuarine channel exemplarily shown for two tidal cycles at mid neap-spring period and discharge of 450 m^3/s. Horizontal white lines indicate instants of slack tide when dune roughness prediction (km 10–55) was activated or deactivated in between tidal phases for asymmetrical dunes (cf. b and d)

3.6 | Stationary bedform roughness induced by ripples

The primary tidal dunes in the Weser estuary retain their shape and asymmetry for periods longer than a tidal cycle. Secondary bedforms, that is, ripples and megaripples partially superimposed to the large compound (tidal) dunes, however, reverse in response to the changing flow direction (e.g., Ernstsen et al., 2011; Lefebvre et al., 2011). These ripples morphologically adapt by redistributing sediment during each tidal phase. We thus assume that ripples and megaripples exert a frictional influence on the flow most of the time during the tidal cycle, since flow energy may be dissipated both during (i) the morphological adaptation when the ripples reverse and (ii) through turbulence as the flow recirculates at the bedform lee side once the ripple is fully reversed and hydraulically effective. Based on this assumption, a simulation with ripple and megaripple bedform roughness prediction (van Rijn, 2007a) was performed from neap to spring tide during 14 tidal cycles to compute the spatiotemporal variation of ripple roughness coefficients considering no bedform hysteresis but equilibrium conditions. By temporal averaging of predicted ripple and megaripple roughness coefficients, a stationary but spatially variable bed roughness was generated. It was then applied as a "stationary ripple roughness" for subsequent simulations in the entire model domain, except for the channelized bed between km 10 and 55 where dune roughness was imposed (Figure 4). Here, ripple-, megaripple-, and dune-induced roughness were predicted dynamically by applying van Rijn's (2007a) empirical formulae dependent on simulated hydrodynamic parameters and sediment characteristics (Section 3.5).

It is noted that Nikuradse roughness heights (k_s) of ripples and megaripples are in the order of a few centimeters and up to a decimeter, respectively. The value of dune-induced roughness is higher than that of ripples and megaripples, in the order of several decimeters, up to the scale of a meter (van Rijn, 2007a).

4 | RESULTS

Dune shape and roughness significantly influence estuarine tidal asymmetry. Small- and large-scale estuarine hydrodynamics and sediment transport are here shown as a proxy for tidal asymmetry.

Figure 5 shows the effects of dune roughness parameterizations on simulated water levels, depth-averaged velocities, and instantaneous bed load sediment transport at an exemplary mid-channel position in the inner estuary (Weser km 33, Elsfleth) for a tidal cycle at mid neap–spring period and discharge of 450 m^3/s. Although a daily inequality exists in the tidal signal, the inferences drawn hereafter are qualitatively valid for the preceding and following tidal cycles (Figure A1, see appendix).

The application of either flood- or ebb-oriented dune roughness parameterizations (FAD or EAD) reveals higher tidal ranges in comparison with symmetrical dunes (SD) (Figure 5a). Overall, the tidal range is highest without the application of dune roughness ("no dunes," ND), that is, bed friction composed of grain, ripple, and megaripple roughness only. Tidal low water is approximately at the same level for ND and FAD, but lower in relation to the level of SD and EAD. For tidal high water, however, SD and FAD have a similar level and are relatively lower than the level of ND and EAD.

Compared with symmetrical dunes, the tidal wave propagates faster up-estuary during flood when imposing ebb-oriented dunes, that is, dune roughness only active during ebb (Figure 5a). Hence, peak flood velocity exceeds peak ebb velocity with a shorter flood than ebb phase (Figure 5b). Likewise, instantaneous bed load

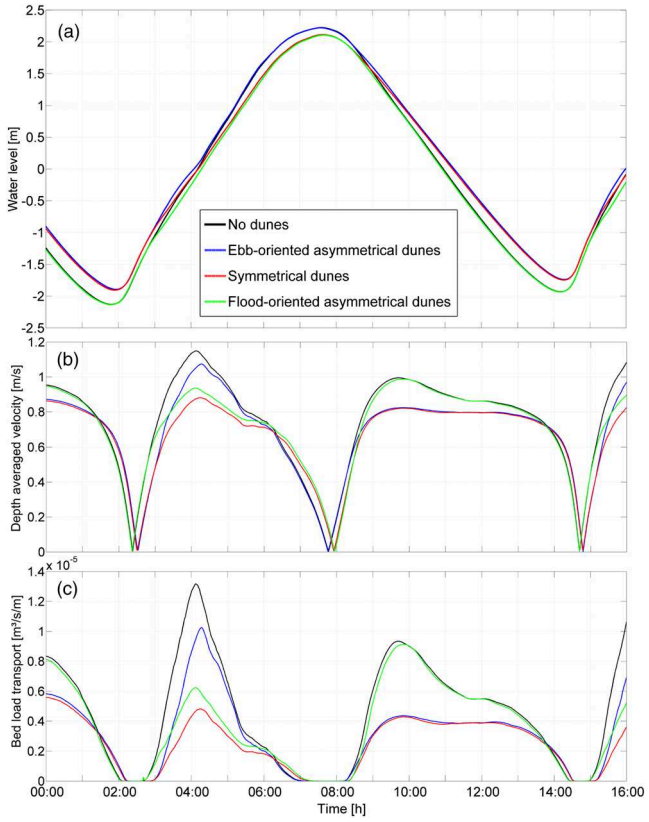

FIGURE 5 Water levels (a), depth-averaged velocities (b), and bed load sediment transports (c) simulated with different bed roughness parameterizations considering "no dunes" (ND), "ebb-oriented asymmetrical" (EAD), "symmetrical" (SD), or "flood-oriented asymmetrical dunes" (FAD) exemplarily shown at Elsfleth (Weser km 33) for a tidal cycle at mid neap-spring period and discharge of 450 m^3/s

sediment transport shows higher peak values during flood than during ebb (Figure 5c).

The opposite results from flood-oriented dunes. The water level rises as fast as for the roughness parameterization of symmetrical dunes, but decreases much faster during ebb (Figure 5a). While symmetrical dunes cause peak flow velocity and peak bed load transport to be similar during ebb and flood, flood-oriented dune roughness causes ebb-dominant peak values. This is because roughness is not active during the ebb phase (Figure 5b,c).

The model run with dune roughness excluded (ND) reveals maximal peak velocity and maximal peak sediment transport of bed material among all scenarios, in particular during the flood.

The residual bed load transport (RBLT) is calculated from the instantaneous bed load flux at intervals of 10 minutes between consecutive low water slack tides of the aforementioned tidal cycle (compare Figure 5c). RBLTs of 5.4×10^{-5}, 1.9×10^{-5}, 5.7×10^{-5}, and 10.3×10^{-5} $m^3/s/m$ for dune roughness parameterizations of ND, EAD, SD, and FAD are all ebb-directed, irrespective of the dune roughness parameterization.

The ratios of ebb to flood peak velocities (peak bed load sediment transports) are determined to be 0.87 (0.71), 0.76 (0.43), 0.93 (0.90), and 1.05 (1.45) for dune roughness parameterizations of ND, EAD, SD, and FAD, respectively. Although peak flood values are higher than peak ebb values (ratio < 1) for ND, EAD, and SD, the tidal asymmetry determined on the basis of residual bed load fluxes is ebb-dominant for all dune roughness scenarios.

4.1 | Along-estuary tidal asymmetry in response to discharge, tidal range, and dune roughness

It can be shown that tidal asymmetry is not uniform along the estuary. Its orientation and strength depend on variable boundary conditions such as tidal energy and freshwater discharge and interact with the frictional effect of bedforms. Normalized residual bed load sediment transport (RBLT) integrated over 14 tidal cycles between neap and spring tides qualitatively shows spatiotemporal effects on tidal asymmetry (Figure 6). A strong variation in RBLT between neap and spring tide (cf. shaded colors spanning an area in Figures 6 and 7) indicates an important influence of tidal range. Likewise, the effect of discharge is evaluated to be important when the variability of RBLT between different discharge regimes is high (Figure 6a–c). The contribution of distinct dune shape parameterizations to the overall effect on tidal asymmetry is estimated from the variation between mean values of RBLT. Six sections (I–VI, illustrated in Figure 6b) along the estuary are identified, revealing characteristic effects on tidal asymmetry, here quantified by direction and magnitude of RBLT.

In section I (km −5 to 5), the amplitude of change of the RBLT is controlled by discharge intensity but also shows a moderate response to different dune roughness parameterizations. Tidal asymmetry is always ebb-directed for enhanced discharges of 450 and 750 m^3/s.

Within section II (km 6–11), RBLT shows no response to discharge, tidal range, or variable dune roughness. Along this section, the harbor basins of the port of Bremen with connection to the estuarine channel are schematized in the model as retention volumes that increase the hydraulically effective cross-section with a consequence of reducing current speeds in the main channel. In addition, 75% of the composition of surface sediments measured and incorporated in the model here is cohesive sediments (Figure 2a). Accordingly, the existing amount of sand to be transported as bed load is reduced abruptly (Figure 6).

In section III (km 12–40), RBLT is highly variable: at a discharge of 150 m^3/s (Figure 6a), tidal asymmetry is flood-dominant for EAD and ebb-dominant for FAD, whereas the net sediment transport for ND and SD is flood-directed at the upper part of this section and turns ebb-directed for the lower part. With increasing discharges of 450 and 750 m^3/s, however, tidal asymmetry becomes increasingly ebb-dominant for all dune roughness parameterizations (Figure 6b,c). The tidal influence, here quantified as the range between neap and spring tide conditions, is largest for EAD, FAD, and ND; exemplarily shown for section III and a discharge regime of 450 m^3/s (Figure 7 is a zoom-in of section III of Figure 6b). With respect to mean and neap tide conditions, spring tide shows increased RBLT in ebb direction for FAD and in flood direction for EAD. Influenced by dune roughness parameterizations of ND and SD, the RBLT reveals a spatially varying response to discharge and tidal range; the prominence of the RBLT of either mean, neap, or spring tide conditions appears to alter along section III (Figure 7). Relative to other dune roughness parameterizations, the frictional effect of symmetrical dunes on RBLT causes the smallest variability between neap and spring tidal conditions along section III.

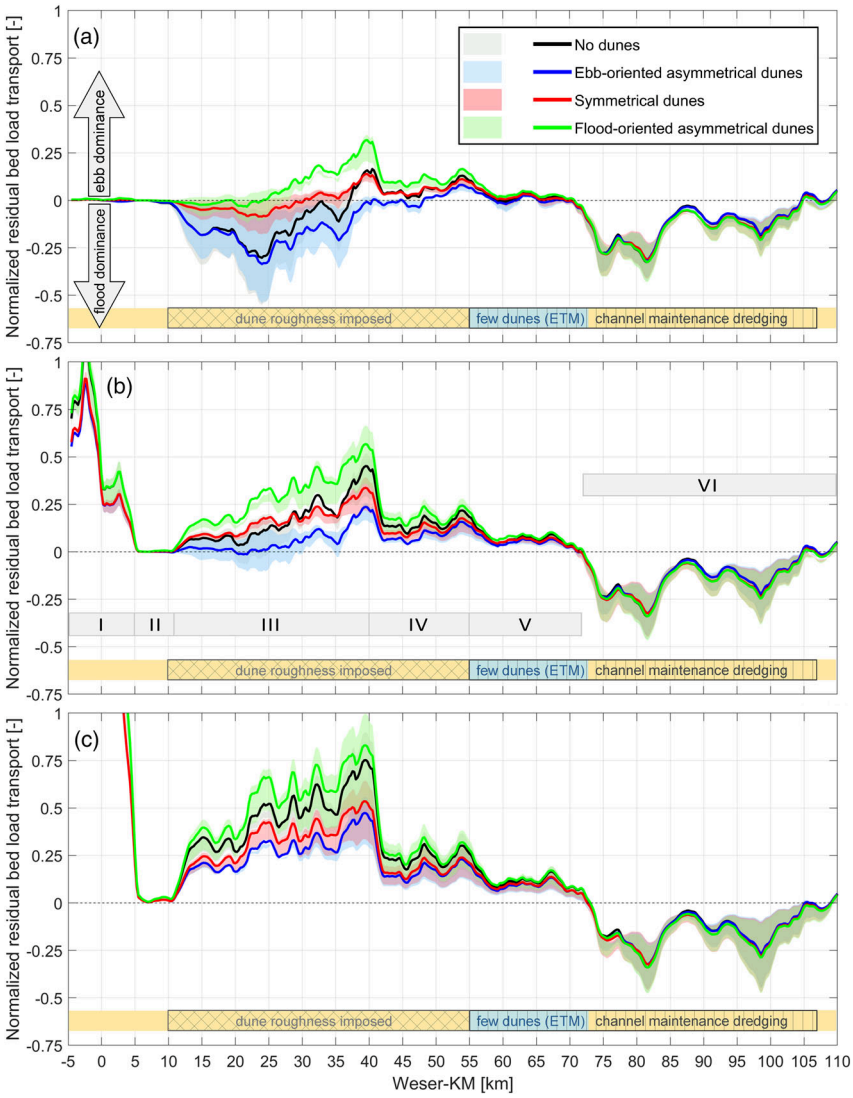

FIGURE 6 Tidal asymmetry quantified by residual bed load sediment transport (RBLT) in response to discharge regimes of (a) 150, (b) 450, and (c) 750 m^3/s, tidal range, and the interaction with distinct dune roughness. Note that positive values reveal ebb dominance. Values are normalized to the spring tide RBLT computed for flood-oriented dune parameterization at a discharge of 750 m^3/s at km 39 (cf. Figure 6c); values > 1 are not presented in the figure. Shaded color patches show the range of RBLT between neap and spring tide conditions. The spatial extent of sections I–VI are depicted by gray rectangles (cf. Figure 6b)

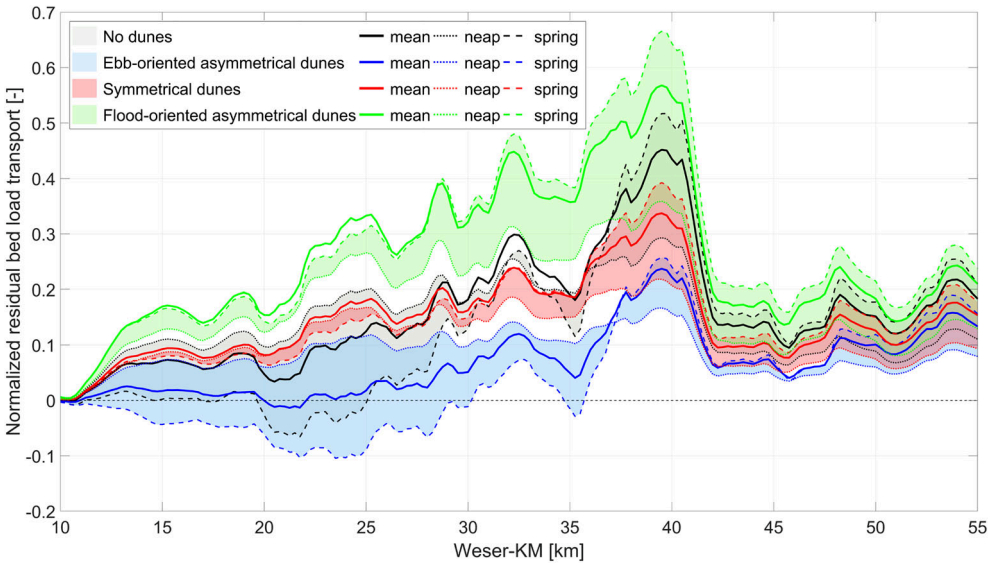

FIGURE 7 This is zoomed in on section III and IV (cf. Figure 6b) to highlight the effect of mean, neap, and spring tidal energy conditions on RBLT for discharge of 450 m^3/s

Between section III and IV, a strong decrease of ebb-dominant RBLT occurs in most cases (Figure 6). This decrease of net sediment transport may be attributed to a combination of a widening of the channelized bed of the fairway downstream of the port of Brake (km 39), but also to a sudden increase of the relative content of cohesive sediments (Figure 2 a).

Tidal asymmetry along section IV (km 41–55) is relatively symmetrical at low discharge, and gets moderately ebb-dominant with

increasing discharge. In analogy to section III, tidally asymmetric dune roughness schematizations EAD and FAD represent the smallest and largest RBLT, respectively.

Section V (km 56–72) covers the estuarine turbidity zone where dune roughness prediction was prevented and only bedform roughness induced by ripples is effective. Tidal asymmetry is generally well balanced: RBLT is small for all simulations and shows the tendency to change from flood to ebb dominance with increasing discharges.

Like in section V, dune roughness was not prescribed at the most downstream section VI (km 73–110). RBLT shows flood dominance; however, there is a tendency to ebb dominance from km 105 to 110 for smaller discharge rates. The effect of tidal range on tidal asymmetry is shown to be strong in section VI.

5 | DISCUSSION

5.1 | Inter-tidal-phase variation of dune roughness

Large tidal bedforms, that is, dunes and sand waves, are shaped by persistent flow conditions, such that their asymmetry is usually assumed to represent the dominant and residual sediment transport direction (e.g., Barnard et al., 2013; Knaapen, 2005). Large tidal dunes in the Weser estuary are quasi morphostatic in view of their hydraulic flow resistance; their overall asymmetric shape and orientation do not reverse with tidal flow direction but are expected to migrate in the dominant flow direction (Nasner, 1977). On timescales of a hydraulic year, however, reversal of tidal dune asymmetry is governed by discharge seasonality, in particular in the upper reach of the Weser estuary (Figure 2e) (Lefebvre et al., 2020). Tidal dunes in the upper reach of the flood dominant Elbe estuary also reverse dune asymmetry and migrate seawards during high-discharge conditions (Zorndt, Wurpts, & Schlurmann, 2011). At the mouth of the Gironde estuary, an opposite dune asymmetry to discharge behavior was observed and explained as a combination of tidal and fluvial changes (Berne et al., 1993).

The present study reveals the overall significance and spatiotemporal effect of dune shape asymmetry on tidal asymmetry. Simulations with bed roughness coefficients parameterizing the hydraulic flow resistance of symmetric and asymmetric dune shapes show substantial small- and large-scale effects on water levels, current velocity, and bed load sediment transport along the estuarine channel. A new aspect of this study is to consider the dependence of asymmetric dune-induced drag. We tested the effect of dune-induced roughness that is hydraulically effective solely in one tidal flow direction for asymmetrical dune shapes (Kwoll et al., 2014; Lefebvre et al., 2013).

A number of studies explored flow resistance of angle-of-repose bedforms, that is, asymmetrical geometries with steep lee-side angles of at least 30° (Best & Kostaschuk, 2002; Kwoll et al., 2016; Lefebvre et al., 2014; Lefebvre & Winter, 2016; Motamedi et al., 2013; Paarlberg et al., 2007). The geometry of natural bedforms and dunes is commonly idealized through triangular shapes. This assumption needs verification for estuarine and tidal dunes. It is not fully understood whether the entire slope of the overall dune lee side or only a short steep segment, often referred to as slip face, governs flow expansion, recirculation, and form drag. Lefebvre et al. (2016) investigated different fluvial dune profiles by categorizing dune lee sides into multiple segments containing steep slip faces and compared their influence on the flow by applying a non-hydrostatic numerical model. Also, the effect of slip faces steeper than 15° on the flow above a natural bedform field was investigated (Lefebvre, 2019). Both studies concluded that predominantly the height and steepness of the slip face and not the bedform height and average lee-side angle alone determine the effective resistance to flow.

The tidal dunes in the upper reach of the Weser estuary (km 20–55) are mostly ebb-oriented asymmetrical (EAD) with average lee-side slopes of 5–10° but with the presence of slip faces with angles typically steeper than 15° (Lefebvre et al., 2020). They are thus assumed to be steep enough to develop at least intermittent flow recirculation and bedform drag. Symmetric and flood-oriented asymmetric dunes are found at the upstream channel during low discharge, but their slopes are most likely too gentle to exert effective flow resistance (Figure 2e). With regard to the here investigated schematic dune roughness scenarios, the effects of EAD on the tidal asymmetry are thus considered as being the most relevant in the Weser estuary.

In nature, residual sediment transport and bedform migration are expected in the dominant flow direction, which may reverse in response to seasonal changes of discharge. At the same time, dune geometry and asymmetry can change and result in different effective roughness. The continuously adapting dune asymmetry and roughness contribute to the estuarine morphodynamic equilibrium. The understanding and formulation of a physically sound and fully dynamic feedback between bedform shape directionality and hydrodynamics is still missing for the semidynamic dune roughness parameterization here applied. Tidal asymmetry is in response to a prescribed dune roughness and discharge regime without a new bedform equilibrium shape being able to establish.

Given the generally unsteady and nonuniform nature of tidal flow, disequilibrium of large compound bedforms, for example, tidal dunes, may be the norm in nature (Myrow et al., 2018). The authors showed that since bedform turnover time is proportional to size, it is likely that the largest dunes in rivers and deserts are always out of equilibrium, and hence, their size and shape do not generally react to the instantaneous flow conditions. Consequently, bedform flow equilibrium is rather unusual and should be taken into consideration in the analysis of bedform evolution and frictional effects of dune roughness on hydrodynamics and sediment transport.

At low freshwater discharge during summer months (100–200 m^3/s), when flood dominance increases relative to periods of high-discharge regime in winter and spring, Weser dunes tend to become symmetrical or even flood-oriented at the upper part of the estuary (Figure 2e). A relative increase of flood dominance during low discharge periods is explained by an unhindered up-estuary propagation of the tidal wave. The flood tide is neither counteracted by ebb-flow enhancing river discharge nor dampened by dune-induced drag. At the beginning of low discharge periods, ebb-oriented dunes still prevail and do not induce flow resistance during flood. Over months of low discharge, dunes then become symmetrical or even flood-oriented.

For this scenario of low discharge (150 m^3/s) and bed roughness parameterization of ebb-oriented dunes (Figure 6 a, blue line)—both being representative for the situation in early summer after high discharges in spring—our idealized model predicts flood-directed net bed load fluxes at the upper estuary, which seems counterintuitive at first given the dunes' ebb-orientation. The residual sediment transport as a

response to the tidal asymmetry is hence interpreted as showing the imbalance of the prescribed boundary conditions, that is, low-discharge regime and ebb-oriented dune shape. The computation of flood-directed residual sediment transport caused by a flood-dominant flow regime may thus be interpreted as the system seeking to change from prescribed ebb-oriented dunes to symmetrical or even flood-oriented dune shapes. The here modeled RBLT and particularly its directionality show the response of the estuarine system, notably the dune field, to changes in river discharge aiming to reach a new morphodynamic equilibrium.

5.2 | Tidal asymmetry influenced by dune-induced friction

Tidal asymmetry and associated effects on residual sediment transport and morphological evolution of estuaries have been extensively discussed (e.g., Dalrymple et al., 2012; De Swart & Zimmerman, 2009; Friedrichs & Aubrey, 1988). For estuarine systems without a tidal weir, tidal energy tends to increase into the estuary but then decreases toward the upper reaches, following a gradual transition to river-dominated flow and sediment transport at the head of the estuary (Dalrymple et al., 2012). Factors for a possible distortion of the tidal wave contributing to the spatial variation of tidal asymmetry may be the interplay with the estuarine basin geometry including channel convergence by changes in width (e.g., Dronkers, 1986), the ratio of tidal wavelength to basin length determining propagating or standing tidal wave characteristics (e.g., Hunt, 1964), areas of intertidal storage influencing tidal propagation speed (e.g., Friedrichs & Aubrey, 1988), density currents (e.g., Burchard et al., 2018), or bed friction owing to the spatially and temporally varying character of sediments, vegetation, or bedforms. In estuaries, many of these factors independently cause flood dominance, that is, shorter rising than falling tides associated with higher flood than ebb velocities, often attributed to the generation of higher-frequency overtides, such as M4/M2 interaction. This flood dominance does not necessarily imply net flood-directed sediment transport, since the dominant direction of RBLT is not only determined by flow intensity but also by the effective duration of transport critical bed shear stress. The peak velocity and the peak bed load transport are higher during the flood than during the ebb for EAD, ND, and SD, respectively, which commonly implies flood dominance. However, the tidal asymmetry determined on the basis of residual bed load fluxes is clearly ebb-dominant for all dune roughness scenarios and discharge of 450 m^3/s (Section 4).

Moreover, other interacting mechanisms can enhance ebb dominance such as Stokes drift return flow (e.g., Dronkers, 1986, 2005; Van der Wegen et al., 2008) or river flow (e.g., Guo et al., 2015b), both promoting ebb-directed net sediment fluxes. Variations in river discharge affect estuarine morphodynamics by supplying sediment, enhancing ebb currents, and dampening flood currents, but foremost through the nonlinear interaction with the propagating tidal wave (Guo et al., 2016; Zhang et al., 2016). Zhang et al. (2016) proposed that the tidal asymmetry is one important "degree of freedom" to allow the estuarine system to seek a state of minimum work by adjusting tidal wave distortion under the influence of varying freshwater discharge. The Weser tidal dunes change shape and asymmetry with varying discharge regime and contribute to the distortion of the tidal wave by inter-tidal-phase varying hydraulic drag. Guo et al. (2016) decomposed the overall tidal asymmetry to identify distinct contributions of riverine discharge, tidal energy, and river–tide interaction, that is, the nonlinear modulation effects of fluvial discharge on tides but without considering the changing patterns of density-driven circulation. The authors further concluded that the flow asymmetry induced by the complex river–tide interaction could be more efficient in favoring ebb-directed residual sediment transport in comparison with the solely river-reinforced residual currents (Guo et al., 2015a). We suspect that the contribution of river–tide interaction decomposed by the authors may comprise the frictional effect of dunes on tidal flow.

Our simulations of varying discharge conditions generally support the coupling effect of discharge and tidal forcing. Tidal distortion and reduction in flood dominance at higher discharge is reflected by increasing ebb-directed residual sediment transport at the inner estuary. At the outer estuary, the interaction of the tidal wave with the basin geometry is assumed to cause flood dominance creating a bed load transport convergence in the middle section of the Weser estuary, as shown by our results.

But foremost, our findings emphasize the additional interaction with distinct dune-induced bed friction, which has been neglected or underestimated in previous analyses of tidal asymmetry. Although schematized, the directionality of different investigated dune profiles reveals an important effect on flow conditions and net transport of bedload material. In section III in the inner estuary, the range of RBLT for different dune shape scenarios is of a similar order of magnitude as the range of RBLT computed for low (150 m^3/s) and high (750 m^3/s) discharge conditions (Figure 6). Hence, the effect of different dune asymmetries on tidal asymmetry is of similar importance as the effect of varying discharge regime on tidal asymmetry.

Guo et al. (2019) further showed the influence of discharge on tidal distortion to increase with tidal range. We found that this relationship to tidal energy is equally affected by the directionality of dune shape and associated tide-dependent bedform roughness. Dune-induced friction during flood is negligible for ebb-oriented dunes enhancing up-estuary propagation and distortion of the tidal wave in inner reaches. An increasing tidal range promotes this distortion, and hence, the variation of RBLT is high between neap and spring tides. The trend is reversed for flood-oriented or symmetrical dune shapes with bedform friction hampering the tidal propagation during flood, reflected by small variation of RBLT between neap and spring tides (Figure 7). The interaction between freshwater discharge and varying tidal range described by Guo et al. (2019) is effective during discharge events only. The interaction between dune shape and varying tidal energy, however, takes place during large parts of the hydraulic year.

Furthermore, density gradients do not play a major role upstream of km 45 in the Weser estuary. Here, baroclinic processes, which dominate tidal dynamics around the location of the estuarine turbidity maximum, are less important. This emphasizes the governing role of spatiotemporal changes of dune roughness and directionality on tidal asymmetry in the upper reach of the estuary.

5.3 | Spatiotemporally varying bedform roughness in estuarine and coastal area models

The frictional influence of the seabed on the flow in tidal environments and, hence, on sediment transport rates and morphological

development is usually schematized by a bed roughness coefficient. Nowadays, it is still common practice to use bed roughness as a general parameter for fine-tuning of numerical models. Adjusting bed roughness coefficients spatially along estuarine channels by calibrating computed water levels and gradients utilizing observations at tidal gauges has been widely used, but neglects inherent physical processes and causes. In practical applications, bed roughness coefficients have often been assigned to vary with water depth to achieve good calibration results (e.g., Cheng et al., 1993; Elias & Hansen, 2013). Common bedform roughness predictors (e.g. van Rijn, 1984, 2007a) may allow for a more realistic, spatially and temporally varying description of the seabed roughness, but still do not account for the bedform alignment with respect to the tidally varying flow direction.

There are only a few studies in which the validity of these predictors has been verified by means of in situ measurements. Davies and Robins (2017) carried out tidal simulations with both constant and spatiotemporally variable bedform roughness at the Menai Strait in Wales, a large tidal channel with connections to the open ocean at both ends. The authors concluded that the dynamic bedform roughness prediction of van Rijn (2007a) performed better in predicting residual water fluxes in the channel than a spatially constant coefficient; the flow was shown to be sensitive in particular to the channel cross-sectional variability of bedform roughness. With respect to measured dune dimensions, the dune roughness and height were overestimated by the model, which was explained by the more symmetrical shape and shorter wavelength of natural tidal bedforms compared with laboratory or idealized bedforms, which was inadequately incorporated in the empirical predictor. Villaret et al. (2011) applied van Rijn's dune roughness predictor in modeling the Gironde and Dee estuaries. At the Gironde estuary, the authors compared observations of water levels and current velocities with two simulations using (i) the dynamic bedform predictor and (ii) applying calibrated temporally invariant roughness coefficients that distinguish only between the inner and outer estuary. The predictor overestimated bedform roughness and flow resistance already at the mouth of the estuary. A possible reason for this overprediction of dune roughness could be sediment grain size being too coarse and uniformly imposed.

In our study, the application of van Rijn's dune roughness predictor was restricted to areas in the Weser model, where dune fields with hydraulically relevant dunes are existent. An unrestricted application, however, showed dune roughness overprediction at the estuarine turbidity maximum and at the mouth of the Weser estuary. Whether this overprediction could be explained by maintenance dredging of the outer channel and cutting of dune crests or by the performance of the predictor applied to tidal environments remains to be investigated.

It is noted that none of these previous studies at tidal environments took account of the asymmetric nature of large tidal dunes and, thus, of inter-tidal-phase varying dune-induced friction.

Our findings reveal a strong sensitivity of tidal asymmetry to the spatiotemporal parameterization of different dune shape configurations at the estuarine scale. Particularly for higher-discharge regimes (Figure 6b,c), simulations taking flow resistance of ebb-oriented dunes into account (e.g., ebb-oriented and symmetrical dunes) lead to significantly smaller residual sediment transport rates at the upper reach and bed load transport convergence at the center of the estuary in comparison with scenario simulations excluding dune roughness parameterization for these ebb-dominant hydrodynamic conditions. Furthermore, although not directly shown for dunes in the outer estuarine channel, the reduction of dune-induced drag on the flow, for example, as a possible effect of outer estuarine channel and dune crest dredging, may enhance the dominance of flood-directed flow and bed load fluxes. These findings are highly relevant to the authorities responsible for maintenance dredging of navigational channels and sediment management in estuaries. Dredging of dune crests inevitably reduces the hydraulic efficiency of dune-induced drag and may increase sediment transport rates. Possible consequences for estuarine systems were delineated by Winterwerp and Wang (2013), who estimated that dredging of dune crests could reduce flow resistance in estuaries, as much as doubling the channel water depth at constant bed roughness. Our results support this by showing net bed load transport to increase when dune roughness decreases.

Additional studies on contrasting tidal environments are necessary before arguing a general recommendation to incorporate time- and space-dependent aspects into the calculation of bedform roughness in coastal-scale numerical models (Brakenhoff et al., 2020a; Brakenhoff et al., 2020b). It is shown to be crucial, however, for coastal settings with large tidal dunes, which preserve their geometry and shape because of an extended morphological response time that is much longer than the semidiurnal tidal cycle. Our investigation denotes an important step in quantifying the influence of asymmetrical dune shapes, which create unidirectional friction, on tidal asymmetry and sediment dynamics at the coastal scale. Further studies need to incorporate the spatiotemporal interaction of bedform roughness directionality with the primary forcing conditions, that is, tides and river discharge, to be fully coupled, allowing investigation of the sensitivity of these factors to long-term morphodynamics. Any such analysis will have to incorporate the spatiotemporal distribution of tidal dune characteristics, obtained from sufficiently long time series of bathymetrical field data (e.g., Krämer et al., 2019; Lefebvre et al., 2020).

6 | CONCLUSION

The present study discusses the effect of different dune shapes and associated dune roughness on tidal asymmetry, quantified by the direction and magnitude of residual bed load sediment transport. The frictional effect of asymmetric and symmetric dune shapes was parameterized through the modified application of a dune roughness predictor (van Rijn, 2007a) in a process-based sediment transport model of the Weser estuary. This new approach focused on tidal-phase-dependent bedform roughness induced by dune asymmetry. It was shown how tidal asymmetry depends on dune flow resistance interacting on spatiotemporal scales with the combined influence of discharge and tidal energy. Our idealized model study revealed that shape and alignment of tidal dunes and associated tide-variable hydraulic resistance substantially affects large-scale estuarine hydrodynamics and bed load fluxes in particular at the inner estuary, upstream of the estuarine turbidity maximum.

In the case of ebb-oriented asymmetric dunes, which exert flow resistance during ebb only, the tidal wave propagates faster upestuary compared with the case of symmetric dunes, that is, flow

resistance during both ebb and flood. Therefore, at very low river discharge, the presence of ebb-oriented dunes can promote flood dominance at the upper estuary, with higher velocities, shorter tidal phase, and enhanced bed load sediment transport during the flood than during the ebb. For higher-discharge regimes, however, the tidal asymmetry becomes ebb-dominant for ebb-oriented dunes.

At the outer Weser estuary, spatiotemporal observations reveal dunes to have low lee-side angles that exert negligible flow resistance. There is little response to discharge, and residual sediment transport is largely flood-directed irrespective of the dune roughness that was prescribed only at the upper estuary. The reduction of dune-induced drag on the flow, for example, as a possible effect of outer estuarine channel and dune crest dredging, is supposed to increase flood-directed net bed load fluxes. This may promote the convergence of large-scale net bed load transport patterns at the center of the estuary.

The interaction of dune shape, discharge, and tidal energy is shown to be complex. Contributions of the interacting processes have been discussed. The effect of different dune asymmetries on tidal asymmetry is of a similar importance as influences of seasonal discharge variability on tidal asymmetry. Our study suggests that the nonequilibrium nature of large asymmetric dunes in tidal flow is critical to tidal asymmetry and large-scale residual bed load transport and needs to be addressed through inter-tidal-phase varying bedform roughness in numerical models covering estuarine and coastal environments.

ACKNOWLEDGMENTS

This study is funded by the research project FAUST, For An improved Understanding of Sediment Transport in Estuaries, financed by and conducted in cooperation with the German Federal Waterways Engineering and Research Institute (BAW). Alice Lefebvre is funded by the German Research Foundation (DFG), project number 345915838. Marius Becker is funded by Kiel Marine Science (KMS). We thank the relevant authorities (Wasserstraßen- und Schifffahrtsamt Weser-Jade-Nordsee) for providing bathymetric field data.

Finally, the authors are grateful to both reviewers, the special issue editor, and the chief editor for their careful reading of the manuscript, their valuable comments, and appreciated suggestions.

CONFLICT OF INTEREST

The authors declare that they do not have any conflicts of interest.

AUTHOR CONTRIBUTIONS

Please find below the contribution of authors in relation to (a) conceptualization, (b) funding acquisition, (c) methodology (including methodological development), (d) investigation (e.g., data collection), (e) resources (provision of data, etc.), (f) software (its provision and development), (g) supervision, (h) writing—initial draft, and (i) writing—reviewing and editing.

G. Herrling: acdhi.

M. Becker: aei.

A. Lefebvre: aei.

A. Zorndt: ei.

K. Krämer: ei.

C. Winter: abi.

DATA AVAILABILITY STATEMENT

We are not allowed to share the original bathymetrical data collected by the local Waterways and Shipping Authorities of Bremen and Bremerhaven. If the paper will be accepted for publication at ESPL, we will share processed data of dune parameters to the fully curated data repository PANGAEA (www.pangaea.de).

ORCID

Gerald Herrling https://orcid.org/0000-0003-0530-8752
Marius Becker https://orcid.org/0000-0001-5469-2506
Alice Lefebvre https://orcid.org/0000-0002-9234-8279
Knut Krämer https://orcid.org/0000-0002-4259-3989
Christian Winter https://orcid.org/0000-0002-8043-2131

REFERENCES

Barnard, P.L., Erikson, L.H., Elias, E.P.L. & Dartnell, P. (2013) Sediment transport patterns in the San Francisco Bay Coastal System from cross-validation of bedform asymmetry and modeled residual flux. *Marine Geology*, 345, 72–95. https://doi.org/10.1016/j.margeo.2012.10.011 [online] Available from: http://linkinghub.elsevier.com/retrieve/pii/S0025322712002344 Accessed 6 January 2015.

Becker, M., Schrottke, K., Bartholomä, A., Ernstsen, V., Winter, C. & Hebbeln, D. (2013) Formation and entrainment of fluid mud layers in troughs of subtidal dunes in an estuarine turbidity zone. *Journal of Geophysical Research, Oceans*, 118(4), 2175–2187. https://doi.org/10.1002/jgrc.20153.

Berne, S., Castaing, P., Le Drezen, E. & Lericolais, G. (1993) Morphology, internal structure, and reversal of asymmetry of large subtidal dunes in the entrance to Gironde Estuary (France). *Journal of Sedimentary Petrology*, 63, 780–793. https://doi.org/10.1306/D4267C03-2B26-11D7-8648000102C1865D [online] Available from: https://pubs.geoscienceworld.org/jsedres/article/63/5/780-793/98462.

Best, J. & Kostaschuk, R.A. (2002) An experimental study of turbulent flow over a low-angle dune. *Journal of Geophysical Research*, 107, 3135. https://doi.org/10.1029/2000jc000294.

Blondeaux, P. (2012) Sediment mixtures, coastal bedforms and grain sorting phenomena: An overview of the theoretical analyses. *Advances in Water Resources*, 48, 113–124. https://doi.org/10.1016/j.advwatres.2012.02.004 [online] Available from: http://linkinghub.elsevier.com/retrieve/pii/S0309170812000346 Accessed 23 September 2013.

Brakenhoff, L., Kleinhans, M., Ruessink, G. & Vegt, M. (2020a) Spatio-temporal characteristics of small-scale wave–current ripples on the Ameland ebb-tidal delta. *Earth Surface Processes and Landforms*, 45, 1248–1261. https://doi.org/10.1002/esp.4802 Accessed 21 January 2020.

Brakenhoff, L., Schrijvershof, R., van der Werf, J., Grasmeijer, B., Ruessink, G. & van der Vegt, M. (2020b) From ripples to large-scale sand transport: The effects of bedform-related roughness on hydrodynamics and sediment transport patterns in delft3d. *Journal of Marine Science and Engineering*, 8(11), 1–25. https://doi.org/10.3390/jmse8110892.

Burchard, H., Hetland, R.D., Schulz, E. & Schuttelaars, H.M. (2011) Drivers of residual estuarine circulation in tidally energetic estuaries: Straight and irrotational channels with parabolic cross section. *Journal of Physical Oceanography*, 41(3), 548–570. https://doi.org/10.1175/2010JPO4453.1.

Burchard, H., Schuttelaars, H.M. & Ralston, D.K. (2018) Sediment trapping in estuaries. *Annual Review of Marine Science*, 10(1), 371–395. https://doi.org/10.1146/annurev-marine-010816-060535.

Cheng, R.T., Casulli, V. & Gartner, J.W. (1993) Tidal, Residual, Intertidal Mudflat (TRIM) model and its applications to San Francisco Bay, California. *Estuarine, Coastal and Shelf Science*, 36, 235–280. https://doi.org/10.1006/ecss.1993.1016 [online] Available from: https://linkinghub.elsevier.com/retrieve/pii/S0272771483710164.

Dalrymple, R.W., Mackay, D.A., Ichaso, A.A. & Choi, K.S. (2012) Processes, morphodynamics, and facies of tide-dominated estuaries. In: *Principles of Tidal Sedimentology*. Dordrecht: Springer Netherlands, pp. 79–107.

Davies, A.G. & Robins, P.E. (2017) Residual flow, bedforms and sediment transport in a tidal channel modelled with variable bed roughness. *Geomorphology*, 295, 855–872. https://doi.org/10.1016/j.geomorph.2017.08.029.

De Swart, H.E. & Zimmerman, J.T.F. (2009) Morphodynamics of tidal inlet systems. *Annual Review of Fluid Mechanics*, 41(1), 203–229. https://doi.org/10.1146/annurev.fluid.010908.165159 (Accessed 30 September 2013.

Deltares. (2014) *Delft3D-FLOW, user manual, simulation of multi-dimensional hydrodynamic flows and transport phenomena, including sediments*. The Netherlands. Deltares, https://content.oss.deltares.nl/delft3d/manuals/Delft3D-FLOW_User_Manual.pdf.

Dronkers, J. (2005) Tide-Topography Interaction. In: *Dynamics of Coastal Systems*. Advanced Series on Ocean Engineering. Vol. 25. World Scientific, pp. 197–324. https://doi.org/10.1142/9789812775252_0004

Dronkers, J. (1986) Tidal asymmetry and estuarine morphology. *Netherlands Journal of Sea Research*, 20(2-3), 117–131. https://doi.org/10.1016/0077-7579(86)90036-0.

Elias, E.P.L. & Hansen, J.E. (2013) Understanding processes controlling sediment transports at the mouth of a highly energetic inlet system (San Francisco Bay, CA). *Marine Geology*, 345, 207–220. https://doi.org/10.1016/j.margeo.2012.07.003 [online] Available from: http://www.sciencedirect.com/science/article/pii/S0025322712001430.

Engelund, F. & Fredsoe, J. (1982) Hydraulic theory of alluvial rivers. *Advances in Hydroscience*, 13, 187–215. https://doi.org/10.1016/B978-0-12-021813-4.50009-3.

Ernstsen, V.B., Lefebvre, A., Bartholdy, J., Bartholomä, A. & Winter, C. (2011) Spatiotemporal height variations of large-scale bedforms in the Grådyb tidal inlet channel (Denmark): a case study on coastal system impact. *Journal of Coastal Research, SI*, 64, 746–750.

Friedrichs, C.T. & Aubrey, D.G. (1988) Non-linear tidal distortion in shallow well-mixed estuaries: a synthesis. *Estuarine, Coastal and Shelf Science*, 27, 521–545. https://doi.org/10.1016/0272-7714(88)90082-0.

Grabemann, I. & Krause, G. (1989) Transport processes of suspended matter derived from time series in a tidal estuary. *Journal of Geophysical Research*, 94, 14373. https://doi.org/10.1029/JC094iC10p14373.

Guo, L., van der Wegen, M., Jay, D.A., Matte, P., Wang, Z.B., Roelvink, D. & He, Q. (2015a) River-tide dynamics: Exploration of nonstationary and nonlinear tidal behavior in the Yangtze River estuary. *Journal of Geophysical Research, Oceans*, 120, 3499–3521. https://doi.org/10.1002/2014JC010491.

Guo, L., van der Wegen, M., Roelvink, D.(.J.A.)., Wang, Z.B. & He, Q. (2015b) Long-term, process-based morphodynamic modeling of a fluvio-deltaic system, part I: The role of river discharge. *Continental Shelf Research*, 109, 95–111. https://doi.org/10.1016/j.csr.2015.09.002 [online] Available from: http://www.sciencedirect.com/science/article/pii/S0278434315300546.

Guo, L., Wang, Z.B., Townend, I. & He, Q. (2019) Quantification of tidal asymmetry and its nonstationary variations. *Journal of Geophysical Research, Oceans*, 124, 773–787. https://doi.org/10.1029/2018JC014372.

Guo, L., Wegen, M., Wang, Z.B., Roelvink, D. & He, Q. (2016) Exploring the impacts of multiple tidal constituents and varying river flow on long-term, large-scale estuarine morphodynamics by means of a 1-D model. *Journal of Geophysical Research - Earth Surface*, 121(5), 1000–1022. https://doi.org/10.1002/2016JF003821.

Hagen, R., Freund, J., Plüß, A., Ihde, R. (2019). Validierungsdokument EasyGSH-DB Nordseemodell. Teil. UnTRIM2 – SediMorph – UnK. Bundesanstalt für Wasserbau (Ed). [online] Available from: https://doi.org/10.18451/k2_easygsh_1

Hendershot, M.L., Venditti, J.G., Bradley, R.W., Kostaschuk, R.A., Church, M. & Allison, M.A. (2016) Response of low-angle dunes to variable flow. *Sedimentology*, 63(3), 743–760. https://doi.org/10.1111/sed.12236.

Herrling, G., Becker, M., Krämer, K., Lefebvre, A., Winter, C. (2019). Parametrization of bedform induced hydraulic flow resistance in coastal-scale numerical models—an evaluation of Van Rijn's empirical bedform roughness predictors. MARID VI. Int. Conf. on Marine and River Dune Dynamics pp. [online] Available from: https://www.marum.de/Binaries/Binary18522/MARIDVI-Herrling-Gerald.pdf

Herrling, G., Benninghoff, M., Zorndt, A., Winter, C. (2017). Drivers of channel-shoal morphodynamics at the Outer Weser estuary. Coastal Dynamics Conference, Helsingoer, Denmark. pp. [online] Available from: http://coastaldynamics2017.dk/onewebmedia/261_herrling.pdf

Hunt, J.N. (1964) Tidal oscillations in estuaries. *Geophysical Journal International*, 8, 440–455. https://doi.org/10.1111/j.1365-246X.1964.tb03863.x.

Julien, P.Y. & Klaassen, G.J. (1995) Sand-dune geometry of large rivers during floods. *Journal of Hydraulic Engineering*, 121(9), 657–663. https://doi.org/10.1061/(ASCE)0733-9429(1995)121:9(657).

Karim, F. (1999) Bed-form geometry in sand-bed flows. *Journal of Hydraulic Engineering*, 125, 1253–1261. https://doi.org/10.1061/(ASCE)0733-9429(1999)125:12(1253).

Knaapen, M.A.F. (2005) Sandwave migration predictor based on shape information. *Journal of Geophysical Research: Earth Surface*, 110(F4). https://doi.org/10.1029/2004JF000195.

Kostaschuk, R. & Best, J. (2005) Response of sand dunes to variations in tidal flow: Fraser Estuary, Canada. *Journal of Geophysical Research: Earth Surface*, 110(F4). https://doi.org/10.1029/2004JF000176.

Krämer, K., Lefebvre, A., Becker, M., Herrling, G., Winter, C. (2019). Long-term dune dynamics in the Lower Weser Estuary. MARID VI. Int. Conf. on Marine and River Dune Dynamics pp. [online] Available from: https://www.marum.de/Binaries/Binary18527/MARIDVI-Kraemer-Knut.pdf

Kwoll, E., Becker, M. & Winter, C. (2014) With or against the tide: The influence of bed form asymmetry on the formation of macroturbulence and suspended sediment patterns. *Water Resources Research*, 50(10), 7800–7815. https://doi.org/10.1002/2013WR014292.

Kwoll, E., Venditti, J.G., Bradley, R.W. & Winter, C. (2016) Flow structure and resistance over subaquaeous high- and low-angle dunes. *Journal of Geophysical Research - Earth Surface*, 121(3), 545–564. https://doi.org/10.1002/2015JF003637.

Kwoll, E., Winter, C. & Becker, M. (2013) Intermittent suspension and transport of fine sediment over natural tidal bedforms. In: *Coherent Flow Structures at Earth's Surface*. Chichester, UK: John Wiley & Sons, Ltd, pp. 231–242.

Lefebvre, A. (2019) Three-dimensional flow above river bedforms: Insights from numerical modeling of a natural dune field (Río Paraná, Argentina). *Journal of Geophysical Research - Earth Surface*, 124(8), 2241–2264. https://doi.org/10.1029/2018JF004928 (Accessed 23 June 2020.

Lefebvre, A., Ernstsen, V.B. & Winter, C. (2011) Influence of compound bedforms on hydraulic roughness in a tidal environment. *Ocean Dynamics*, 61, 2201–2210. https://doi.org/10.1007/s10236-011-0476-6.

Lefebvre, A., Ernstsen, V.B. & Winter, C. (2013) Estimation of roughness lengths and flow separation over compound bedforms in a natural-tidal inlet. *Continental Shelf Research*, 61-62, 98–111. https://doi.org/10.1016/j.csr.2013.04.030.

Lefebvre, A., Herrling, G., Zorndt, A., Krämer, K., Marius, B., Winter, C. (2020). Tidal bedforms dynamics, Weser River, Germany. Online, 4–8 May 2020, EGU2020–13499 pp.

Lefebvre, A., Paarlberg, A.J., Ernstsen, V.B. & Winter, C. (2014) Flow separation and roughness lengths over large bedforms in a tidal environment: A numerical investigation. *Continental Shelf Research*, 91, 57–69. https://doi.org/10.1016/j.csr.2014.09.001 [online] Available from: http://linkinghub.elsevier.com/retrieve/pii/S027843431400274X.

Lefebvre, A., Paarlberg, A.J. & Winter, C. (2016) Characterising natural bedform morphology and its influence on flow. *Geo-Marine Letters*, 36, 379–393. https://doi.org/10.1007/s00367-016-0455-5 Accessed 18 July 2018.

Lefebvre, A. & Winter, C. (2016) Predicting bed form roughness: The influence of lee side angle. *Geo-Marine Letters*, 36, 121–133. https://doi.org/10.1007/s00367-016-0436-8.

Lesser, G.R., Roelvink, J.A., van Kester, J.A.T.M. & Stelling, G.S. (2004) Development and validation of a three-dimensional morphological

model. *Coastal Engineering*, 51, 883–915. https://doi.org/10.1016/j.coastaleng.2004.07.014 [online] Available from: http://linkinghub.elsevier.com/retrieve/pii/S0378383904000870 Accessed 25 September 2013.

Milbradt, P., Valerius, J. & Zeiler, M. (2015) Das Funktionale Bodenmodell: Aufbereitung einer konsistenten Datenbasis für die Morphologie und Sedimentologie. *Die Küste*, 83, 19–38. [online] Available from: http://vzb.baw.de/die-kueste/0/k083102.pdf.

Motamedi, A., Afzalimehr, H., Gallichand, J. & Fazel Najaf Abadi, E. (2013) Lee angle effects in near bed turbulence: An experimental study on low and sharp angle dunes. *International Journal of Hydraulic Engineering*, 1, 68–74. https://doi.org/10.5923/j.ijhe.20120106.02.

Myrow, P.M., Jerolmack, D.J. & Perron, J.T. (2018) Bedform disequilibrium. *Journal of Sedimentary Research*, 88(9), 1096–1113. https://doi.org/10.2110/jsr.2018.55.

Naqshband, S., Ribberink, J.S., Hurther, D. & Hulscher, S.J.M.H. (2014) Bed load and suspended load contributions to migrating sand dunes in equilibrium. *Journal of Geophysical Research - Earth Surface*, 119, 1043–1063. https://doi.org/10.1002/2013JF003043.

Nasner, H. (1977) Transportmechanismus in Tideriffeln. *Die Küste*, 31, 90–101. https://hdl.handle.net/20.500.11970/101110.

Paarlberg, A.J., Dohmen-Janssen, C.M., Hulscher, S.J.M.H. & Termes, P. (2007) A parameterization of flow separation over subaqueous dunes. *Water Resources Research*, 43(12). https://doi.org/10.1029/2006WR005425.

Paarlberg, A.J., Dohmen-Janssen, C.M., Hulscher, S.J.M.H., Termes, P. & Schielen, R. (2010) Modelling the effect of time-dependent river dune evolution on bed roughness and stage. *Earth Surface Processes and Landforms*, 35(15), 1854–1866. https://doi.org/10.1002/esp.2074.

Sandbach, S.D., Lane, S.N., Hardy, R.J., Amsler, M.L., Ashworth, P.J., Best, J.L., *et al*. (2012) Application of a roughness-length representation to parameterize energy loss in 3-D numerical simulations of large rivers. *Water Resources Research*, 48(12). https://doi.org/10.1029/2011WR011284.

Valerius, J., Kösters, F. & Zeiler, M. (2015) Erfassung von Sandverteilungsmustern zur großräumigen Analyse der Sedimentdynamik auf dem Schelf der Deutschen Bucht. *Die Küste*, 83, 39–63.

van Rijn, L.C. (1984) Sediment transport, part III: Bed forms and alluvial roughness. *Journal of Hydraulic Engineering*, 110, 1733–1754. https://doi.org/10.1061/(ASCE)0733-9429(1984)110:12(1733) Accessed 18 July 2018.

van Rijn, L.C. (2007a) Unified view of sediment transport by currents and waves. I: Initiation of motion, bed roughness, and bed-load transport. *Journal of Hydraulic Engineering*, 133, 649–667. https://doi.org/10.1061/(ASCE)0733-9429(2007)133:6(649).

van Rijn, L.C. (2007b) Unified View of Sediment Transport by Currents and Waves. III: Graded Beds. *Journal of Hydraulic Engineering*, 133(7), 761–775. https://doi.org/10.1061/(asce)0733-9429(2007)133:7(761).

van der Wegen, M., Wang, Z.B., Savenije, H.H.G., Roelvink, J.A. (2008) Long-term morphodynamic evolution and energy dissipation in a coastal plain, tidal embayment. *Journal of Geophysical Research*, 113 (F3). https://doi.org/10.1029/2007jf000898

Vanoni, V.A. & Hwang, L.-S. (1967) Bed forms and friction in streams. *Journal of the Hydraulics Division*, 93(3), 121–144. https://doi.org/10.1061/JYCEAJ.0001607.

Villaret, C., Hervouet, J.-M., Kopmann, R., Merkel, U. & Davies, A.G. (2013) Morphodynamic modeling using the Telemac finite-element system. *Computers & Geosciences*, 53, 105–113. https://doi.org/10.1016/j.cageo.2011.10.004.

Villaret, C., Huybrechts, N., Davies, A. G., Way, O. (2011). Effect of bed roughness prediction on morphodynamic modelling: Application to the Dee estuary (UK) and to the Gironde estuary (France). 1149 pp.

Wang, Y., Yu, Q., Jiao, J., Tonnon, P.K., Wang, Z.B. & Gao, S. (2016) Coupling bedform roughness and sediment grain-size sorting in modelling of tidal inlet incision. *Marine Geology*, 381, 128–141. https://doi.org/10.1016/J.MARGEO.2016.09.004 Accessed 20 July 2018.

Warmink, J.J., Straatsma, M.W., Huthoff, F., Booij, M.J. & Hulscher, S.J.M.H. (2013) Uncertainty of design water levels due to combined bed form and vegetation roughness in the Dutch River Waal. *Journal of Flood Risk Management*, 6(4), 302–318. https://doi.org/10.1111/jfr3.12014.

Winter, C., Lefebvre, A., Benninghoff, M. & Ernstsen, V.B. (2015) Die Verteilung und Eigenschaften von Bodenformen in der Deutschen Bucht, eine Rekonstruktion der Karten von Ulrich (1973). *Die Küste, Archive for Research and Technology on the North Sea and Baltic Coast*, 83, 65–76.

Winterwerp, J.C., Lely, M. & He, Q. (2009) Sediment-induced buoyancy destruction and drag reduction in estuaries. *Ocean Dynamics*, 59(5), 781–791. https://doi.org/10.1007/s10236-009-0237-y.

Winterwerp, J.C. & Wang, Z.B. (2013) Man-induced regime shifts in small estuaries—I: Theory. *Ocean Dynamics*, 63(11-12), 1279–1292. https://doi.org/10.1007/s10236-013-0662-9.

Yalin, M.S. (1964) Geometrical properties of sand wave. *Journal of the Hydraulics Division*, 90, 5105–5119.

Zhang, M., Townend, I., Zhou, Y. & Cai, H. (2016) Seasonal variation of river and tide energy in the Yangtze estuary, China. *Earth Surface Processes and Landforms*, 41(1), 98–116. https://doi.org/10.1002/esp.3790.

Zorndt, A.C., Wurpts, A. & Schlurmann, T. (2011) The influence of hydrodynamic boundary conditions on characteristics, migration, and associated sand transport of sand dunes in a tidal environment. *Ocean Dynamics*, 61(10), 1629–1644. https://doi.org/10.1007/s10236-011-0452-1.

How to cite this article: Herrling, G., Becker, M., Lefebvre, A., Zorndt, A., Krämer, K. & Winter, C. (2021) The effect of asymmetric dune roughness on tidal asymmetry in the Weser estuary. *Earth Surface Processes and Landforms*, 1–18. Available from: https://doi.org/10.1002/esp.5170

APPENDIX A.

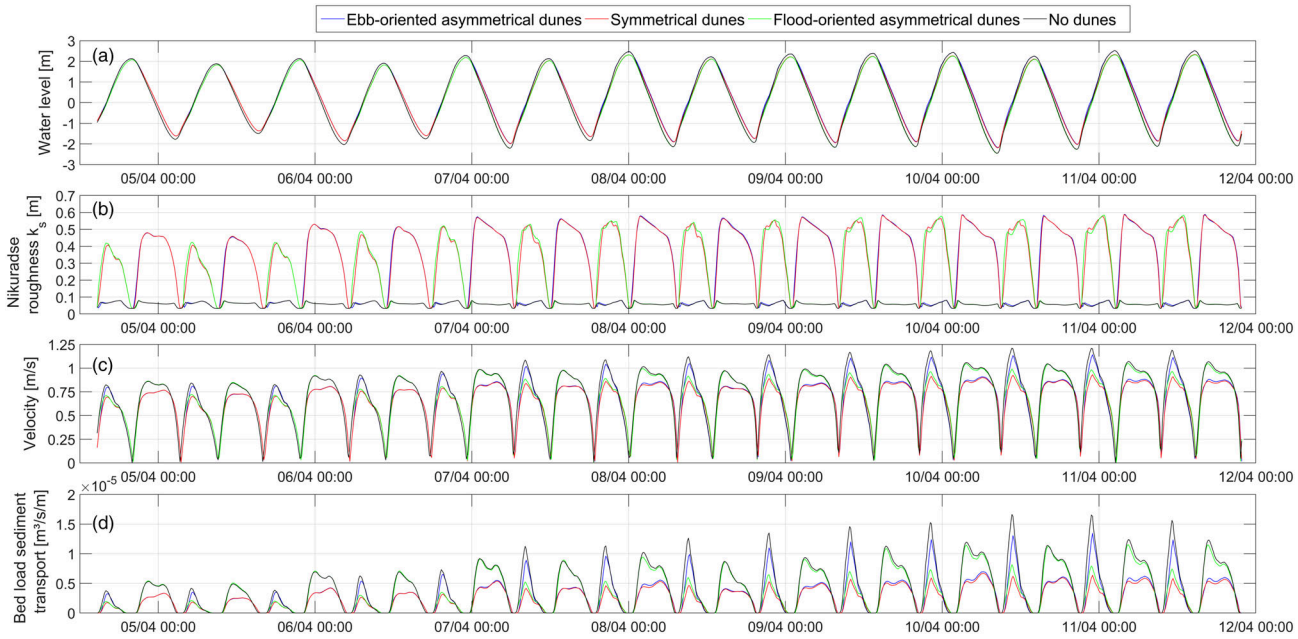

FIGURE A1 Water level (a), combined bed roughness (b), depth-averaged velocity (c), and bed load sediment transport (d) are shown for distinct dune roughness parameterizations at Weser km 33 and discharge of 450 m^3/s

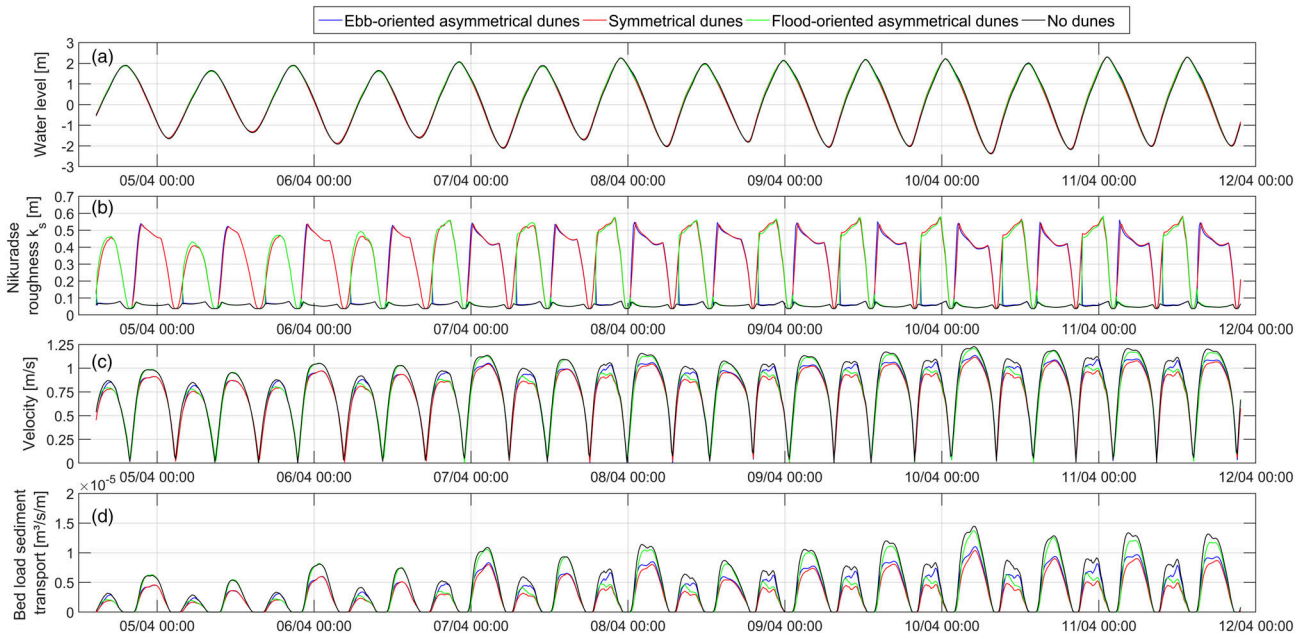

FIGURE A2 Water level (a), combined bed roughness (b), depth-averaged velocity (c), and bed load sediment transport (d) are shown for distinct dune roughness parameterizations at Weser km 54 and discharge of 450 m^3/s

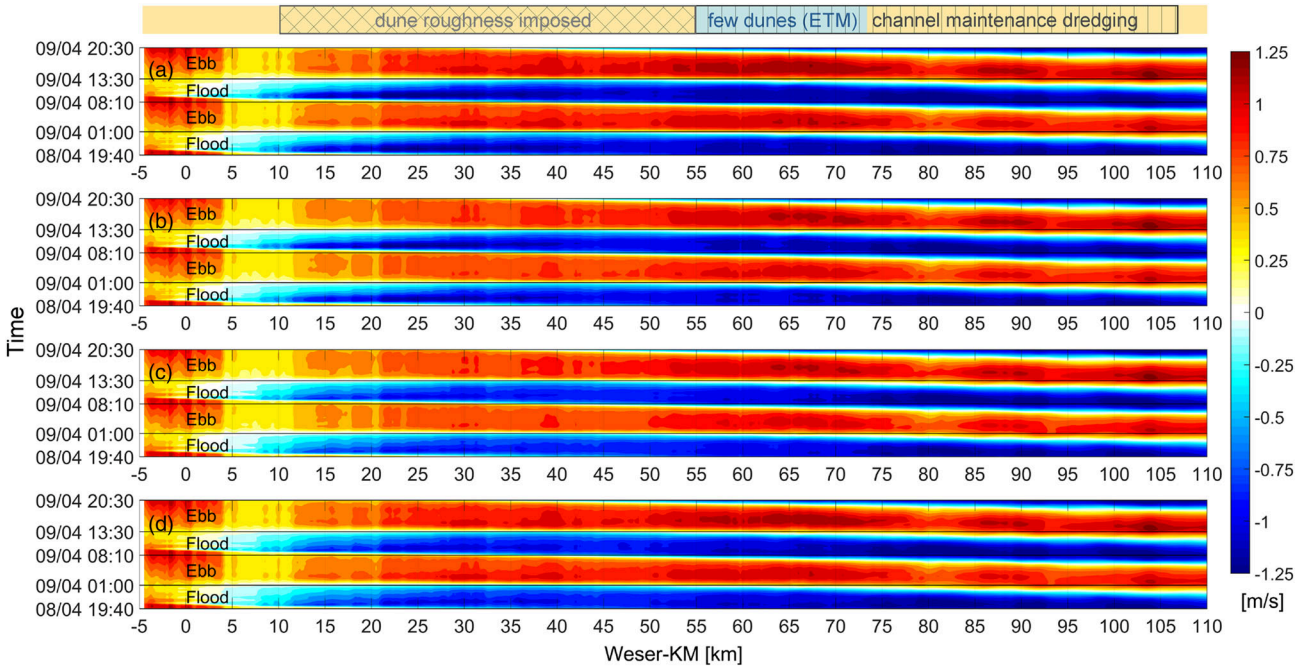

FIGURE A3 Depth-averaged flow velocity for scenario simulations considering "no dunes" (a), "ebb-oriented asymmetrical" (b), "symmetrical" (c), or "flood-oriented asymmetrical dunes" (d) along the estuarine channel exemplarily shown for two tidal cycles at mid neap-spring period and discharge of 450 m^3/s

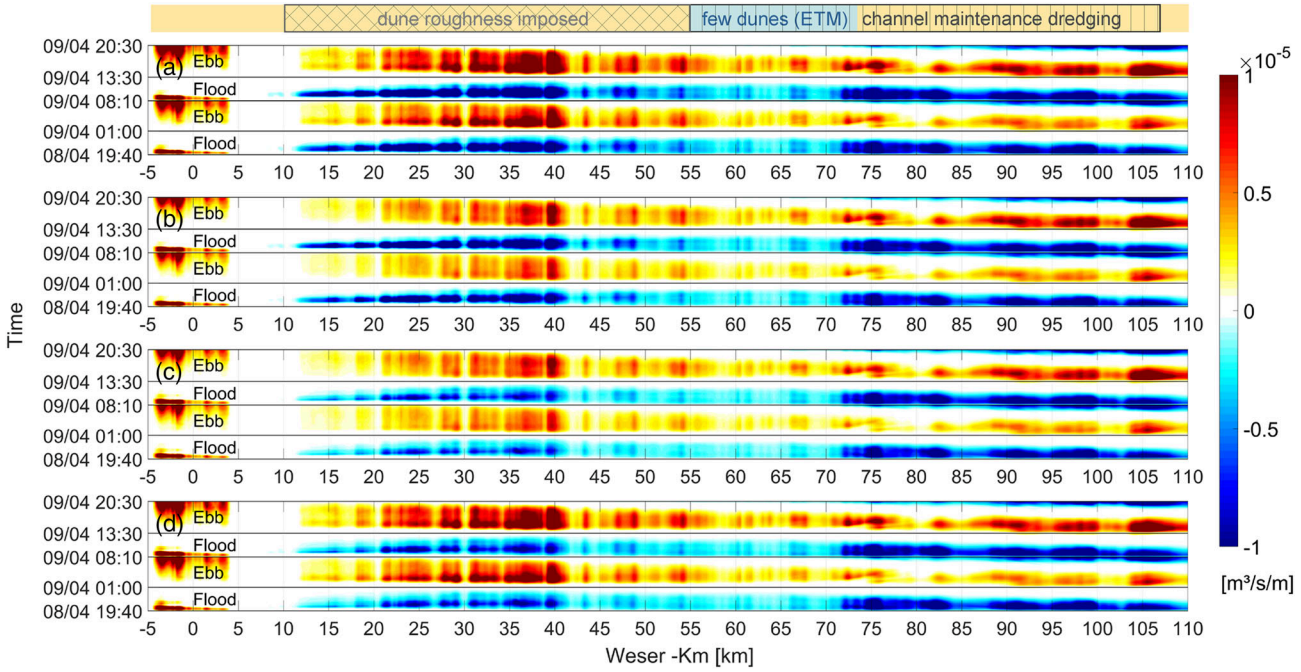

FIGURE A4 Instantaneous bed load sediment transport for scenario simulations considering "no dunes" (a), "ebb-oriented asymmetrical" (b), "symmetrical" (c), or "flood-oriented asymmetrical dunes" (d) along the estuarine channel exemplarily shown for two tidal cycles at mid neap-spring period and discharge of 450 m^3/s